Structure, temporal evolution, and heat flux estimates from the Lucky Strike deep-sea hydrothermal field derived from seafloor image mosaics

Thibaut Barreyre and Javier Escartín

Marine Geosciences Group, Institut de Physique du Globe de Paris, CNRS, UMR 7154–Univ. Paris Diderot, Sorbonne Paris Cité, Paris CEDEX 5, France (barreyre@ipgp.fr)

Rafael Garcia

Computer Vision and Robotics Group, University of Girona, Girona E–17001, Spain

Mathilde Cannat

Marine Geosciences Group, Institut de Physique du Globe de Paris, CNRS, UMR 7154–Univ. Paris Diderot, Sorbonne Paris Cité, Paris CEDEX 5, France

Eric Mittelstaedt

Woods Hole Oceanographic Institution, Woods Hole, Massachusetts 02543, USA

Ricard Prados

Computer Vision and Robotics Group, University of Girona, Girona E–17001, Spain

[1] Here we demonstrate with a study of the Lucky Strike hydrothermal field that image mosaicing over large seafloor areas is feasible with new image processing techniques, and that repeated surveys allow temporal studies of active processes. Lucky Strike mosaics, generated from >56,000 images acquired in 1996, 2006, 2008 and 2009, reveal the distribution and types of diffuse outflow throughout the field, and their association with high-temperature vents. In detail, the zones of outflow are largely controlled by faults, and we suggest that the spatial clustering of active zones likely reflects the geometry of the underlying plumbing system. Imagery also provides constraints on temporal variability at two time-scales. First, based upon changes in individual outflow features identified in mosaics acquired in different years, we document a general decline of diffuse outflow throughout the vent field over time-scales up to 13 years. Second, the image mosaics reveal broad patches of seafloor that we interpret as fossil outflow zones, owing to their association with extinct chimneys and hydrothermal deposits. These areas encompass the entire region of present-day hydrothermal activity, suggesting that the plumbing system has persisted over long periods of time, loosely constrained to hundreds to thousands of years. The coupling of mosaic interpretation and available field measurements allow us to independently estimate the heat flux of the Lucky Strike system at ∼200 to 1000 MW, with 75% to >90% of this flux taken up by diffuse hydrothermal outflow. Based on these heat flux estimates, we propose that the temporal decline of the system at short and long time scales may be explained by the progressive cooling of the AMC, without replenishment. The results at Lucky Strike demonstrate that repeated image surveys can be routinely performed to characterize and study the temporal variability of a broad range of vent sites hosting active processes (e.g., cold seeps, hydrothermal fields, gas outflows, etc.), allowing a better understanding of fluid flow dynamics from the sub-seafloor, and a quantification of fluxes.

1. Introduction

[2] Hydrothermal activity along mid-ocean ridges accounts for ∼30% (∼11 TW) of the oceanic heat flux (∼32 TW), and is therefore responsible for approximately ∼25% of the Earth's heat loss (∼43 TW) [*Stein and Stein*, 1994; *Elderfield and Schultz*, 1996]. Convection of fluids in the lithosphere is driven by heat sources at depth (magma bodies, hot lithospheric material, exothermic reactions [e.g., *Wilcock and Delaney*, 1996; *Emmanuel and Berkowitz*, 2006]), and plays a major role in oceanic crust formation on-axis. The dynamics of these systems depends on numerous parameters, including the presence of tectonic features (i.e., faults and cracks) acting as fluid pathways, the physical properties of the substrate (porosity, permeability), and the nature and distribution of heat sources, as well as temporal variability (seismicity, magmatic injections, lithospheric thermal evolution). Fluid discharge at the seafloor often occurs in well-defined hydrothermal fields that extend over areas of up to ∼1 km^2, along mid-ocean ridges [e.g., *German et al.*, 2010a]. The nature and geometry of fluid recharge at hydrothermal systems is poorly known, but assumed to occur over a broader area than that of the discharge zone (e.g., along faulted zones flanking the ridge axis) [*Lister*, 1982; *Alt*, 1995; *Wilcock and Delaney*, 1996]. The focusing of hydrothermal discharge is most extreme at slow-spreading ridges [*Fontaine and Wilcock*, 2007], where sites are larger and associated with higher heat fluxes than those along intermediate- and fast spreading ridges [*Baker*, 2007].

[3] Two major types of hydrothermal outflow are often distinguished: a) focused, high temperature (>300°C) vents [*Spiess et al.*, 1980; *Von Damm*, 1990] and b) diffuse flow [*Baker et al.*, 1993; *Fisher and Becker*, 1991; *Trivett and Williams*, 1994] at temperatures that vary from a few degrees above ambient seawater to ∼150°C. The partitioning of heat flux between diffuse and focused flow is variable, from sites showing no apparent diffuse flow (e.g., Rainbow [*German et al.*, 2010b]), to sites with diffuse flow taking from 50% [e.g., *Veirs et al.*, 2006] up to 90% [e.g., *Schultz et al.*, 1992; *Ramondenc et al.*, 2006] of the heat flux. These disparities likely reflect fundamental differences in the subsurface outflow structure associated with discharge zones, impacting on the mixing of cold seawater and hydrothermal fluids.

[4] To date, the extent of diffuse outflow is poorly constrained, owing to the fact that hydrothermal sites are characterized largely through visual observations during ROV and submersible dives, providing only local and partial information, and in the absence of systematic image seafloor surveys. The first of such surveys was carried out in 1976, and provided sparse coverage along the FAMOUS segment (Mid-Atlantic Ridge) [*Brundage and Patterson*, 1976]. The first optical mapping of hydrothermal fields was conducted with the ARGOII deep-towed system at the TAG and Lucky Strike fields [*Kleinrock and Humphris*, 1996; *Humphris et al.*, 2002]. Recent developments in image acquisition techniques and underwater vehicles have allowed a wide range of new seafloor studies (e.g., archeology [*Foley et al.*, 2009], seeps [*Valentine et al.*, 2010; *Lessard-Pilon et al.*, 2010], asphalt flows [*Brüning et al.*, 2010], whale falls [*Lundsten et al.*, 2010], as well as hydrothermal fields [*Maki et al.*, 2008]). However, all these more recent surveys are limited to a small surface area (e.g., 10,000 m^2 [*Maki et al.*, 2008]), and thus not well adapted to map a complete hydrothermal field such as that of Lucky Strike. In recent years, we have developed new image-processing techniques [*Escartín et al.*, 2008a; *Garcia et al.*, 2011; *Prados et al.*, 2011] tailored to map large areas of up to 1 km^2 or more, thus expanding the possible applications for seafloor image surveying and their quantitative interpretation.

[5] For the first time, we present a systematic image mapping of a complete hydrothermal field, at the Lucky Strike segment along the Mid-Atlantic Ridge (MAR), one of the largest and best-known deep-sea systems of its kind (see Section 2). Here, the hydrothermal outflow is located at the segment center [*Langmuir et al.*, 1997], overlying a 3-km deep magma chamber [*Singh et al.*, 2006], and along an axial extensional graben at the summit of a central volcano. The image mosaics, generated using new image processing techniques, together with ground-truthing from submersible dives, constrain the surface structure, nature, and distribution of active hydrothermal venting throughout the whole Lucky Strike hydrothermal site. In contrast, discrete observations at individual sites (e.g., visual inspection with remotely operated vehicles – ROVs - or submersibles) preclude the type of comprehensive characterization of the seafloor that image mosaics provide. Prior studies have suggested an association between hydrothermal outflow and small-scale tectonic features (faults, fissures), both at the Lucky Strike hydrothermal field [*Ondréas et al.*, 2009] and elsewhere [*Haymon et al.*, 2005; *Bohnenstiehl and Kleinrock*, 2000a, 2000b]; this association to tectonic structures is also found within well-developed fault zones (e.g., oceanic detachments [e.g., *McCaig et al.*, 2007; *Escartín et al.*, 2008b]). Mosaic interpretation allow us to evaluate and quantify this association between hydrothermal outflow and faulting, while constraining the overall distribution of active venting. We propose that the outflow geometry derived from the image mosaics can be used to infer the geometry of underlying plumbing system. Furthermore, repeated surveys reveal change in hydrothermal activity at time-scales of 1 to 13 years at the Lucky Strike site, while their geological interpretation indicates variability at longer time scales (100 s to 1000 s of years?). We combine the mosaic interpretation with available field measurements of fluid flow and temperature to provide an estimate of heat flux, which is independent of estimates based on water column studies yielding fluxes of 100 to ~4000 MW [*Wilson et al.*, 1996; *Jean-Baptiste et al.*, 1998], and its partition between focused and diffuse flow.

2. Geological Setting of the Lucky Strike Segment and Hydrothermal Field

[6] The ~80 km long Lucky Strike ridge segment extends along the Mid-Atlantic Ridge between 37°03′N and 37°37′N (Figure 1a), is located ~400 km southwest of the Azores Islands, and spreads at a full rate of ~22 mm/yr [*DeMets et al.*, 1990; *Cannat et al.*, 1999]. It has a well-developed rift valley with a central volcano underlain by a 3-km deep axial magma chamber (AMC) [*Singh et al.*, 2006; *Combier*, 2007] (Figures 1b and 1c). The volcano summit hosts the Lucky Strike field (LS), with hydrothermal activity surrounding a fossil lava lake [*Fouquet et al.*, 1995; *Ondréas et al.*, 1997, 2009; *Humphris et al.*, 2002], and associated with a local low in seafloor magnetization [*Miranda et al.*, 2005] likely due to basalt alteration [*Tivey and Johnson*, 2002]. Discovered during the 1992 FAZAR cruise [*Langmuir et al.*, 1993; *Wilson et al.*, 1996], the Lucky Strike hydrothermal field has been extensively studied during recent expeditions (DIVA1 and FLORES, 1994; LUSTRE, 1996; MoMARETO and Graviluck, 2006; MoMAR, 2008; Bathyluck, 2009; MoMARSAT 2010 and 2011), and is the object of long-term monitoring [e.g., *Ballu et al.*, 2009; *Colaço et al.*, 2011], including a seafloor observatory (ESONET-EMSO European project [*Ruhl et al.*, 2011]). Hydrothermal chimneys, mounds, and associated areas of diffuse outflow [*Humphris et al.*, 2002; *Ondréas et al.*, 2009] extend over 1 km². The substrate is primarily basalt, locally overlain by either massive sulfide deposits (NE of the hydrothermal field), or by a hydrothermally cemented breccia forming a 'hydrothermal slab' cap [*Langmuir et al.*, 1997; *Ondréas et al.*, 1997, 2009]. The area is crosscut by numerous normal faults [e.g., *Scheirer et al.*, 2000; *Humphris et al.*, 2002; *Ondréas et al.*, 1997, 2009], associated with a small axial graben (~1 km wide) that runs along the axial valley floor and that dissects the volcano. These faults may operate as outflow conduits, controlling hydrothermal discharge to the seafloor and spatial distribution of main vents [*Ondréas et al.*, 2009]. The geochemistry of hydrothermal fluids reveals a reaction zone whose depth is poorly constrained at 1 km to 3 km [*Charlou et al.*, 2000; *Fontaine et al.*, 2009], but limited to the crust above the AMC. Furthermore, there is both a spatial and limited temporal variability in end-member major elements compositions of the vent fluids, whose origin is not well-understood (e.g., plumbing system, reaction zone at depth). It has been suggested that these reflect two major distinct source waters feeding the southeastern, and the northeastern and western vents [e.g., *Von Damm et al.*, 1998; *Charlou et al.*, 2000]. This site witnessed a possible dike intrusion in 2002, which may have reinvigorated hydrothermal activity as indicated by an apparent and local increase in
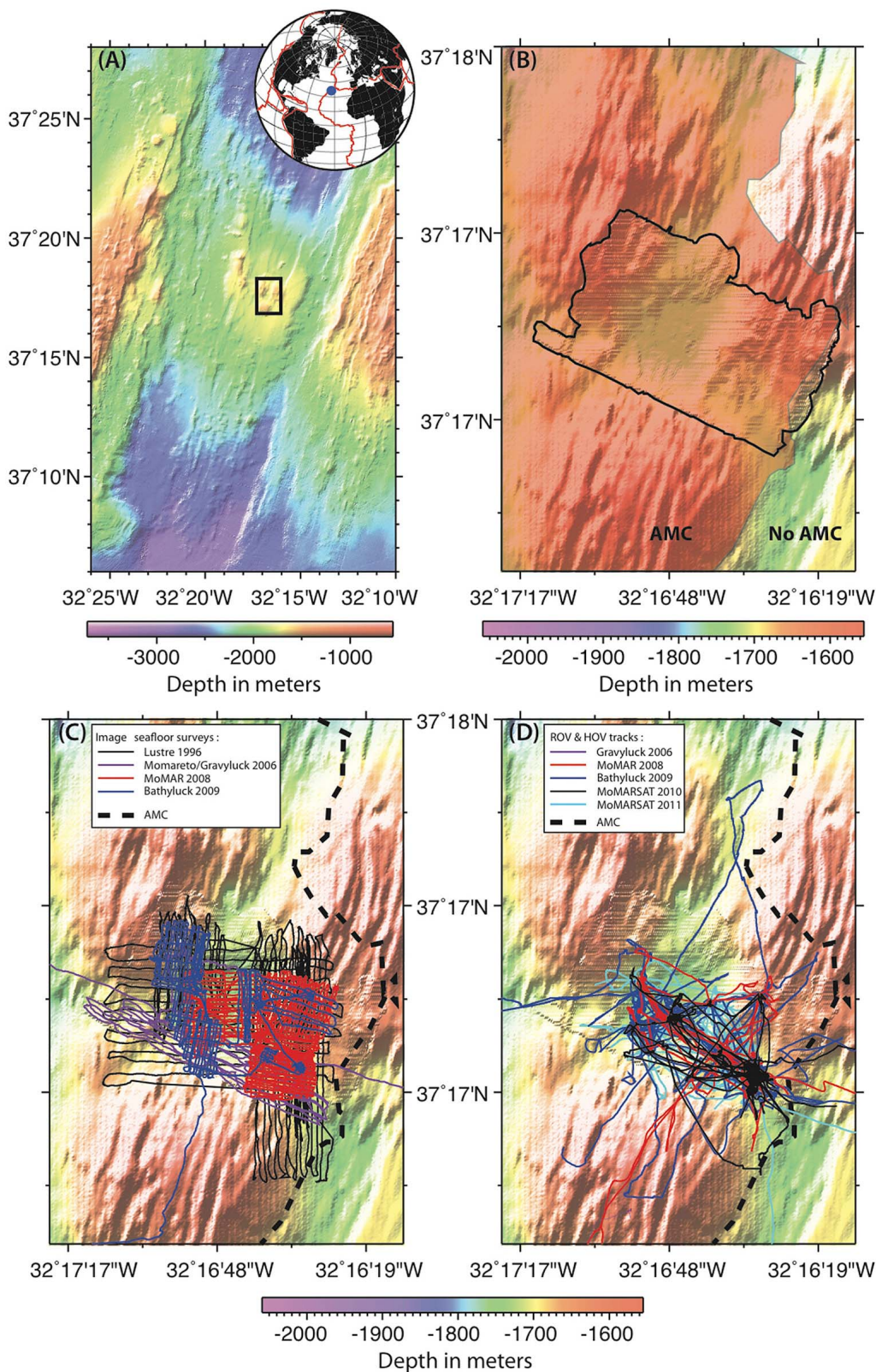
Figure 1

microbial activity observed between 1997 and 2003 [*Dziak et al.*, 2004].

[7] Recent geophysical studies also constrain the nature and properties of the crust above the AMC. Seismic reflection and refraction studies reveal that the crustal volume underlying the hydrothermal field (below the central volcano and above the axial magma chamber) is characterized by a low-velocity anomaly both from refraction and reflection data [*Seher et al.*, 2010a, 2010b], in addition to reflectors that correspond to the main faults developed within the rift valley floor [e.g., *Combier*, 2007; V. Combier et al., Three-dimensional geometry of axial magma chamber roof and faults at Lucky Strike volcano on the Mid-Atlantic Ridge, submitted to *Journal of Geophysical Research*, 2011]. This low-velocity anomaly is interpreted to be due to increased porosity relative to surrounding crust. However, the spatial resolution of these data (~50 m along seismic profiles and >100 m across them for reflection data [*Seher et al.*, 2010b], and >1 km for seismic refraction data [*Seher et al.*, 2010a]) is too coarse to relate the surface distribution of discharge zones to the underlying plumbing system (porosity and fluid contents) below the seafloor.

3. Methodology

3.1. Seafloor Image Surveys

[8] Image surveys of the seafloor at Lucky Strike were carried out in 1996, 2006, 2008, and 2009, using down-looking electronic black-and-white still cameras (Figure 1b). Deep-towed systems were used during the LUSTRE'96 cruise (ARGO II system, WHOI, USA) [*Humphris et al.*, 2002; *Escartín et al.*, 2008a] and the 2006 Graviluck Cruise (TowCam system [*Fornari*, 2003]). A high-sensitivity, black and white electronic still camera (OTUS [*Simeoni et al.*, 2007]) mounted on the ROV VICTOR6000 (IFREMER, France) was used during the Momareto 2006, MoMAR2008, and Bathyluck 2009 cruises. All these surveys focused

on the known active vents at the Lucky Strike hydrothermal field. The 1996 and 2008 surveys were the most extensive throughout the Lucky Strike field, allowing a detailed characterization of actively venting areas, including the spatial distribution of outflow zones, their styles, and their relationship to substrate and structure. The 2006 and 2009 surveys, while more limited, allowed the extension of the area surveyed in 1996 and 2008. These also provided overlap for temporal studies, particularly at well-known and studied sites (e.g., Tour Eiffel and Montsegur vents). The TowCam track across the field (Graviluck 2006) was excluded from this study due to its limited coverage and overlap with the other surveys (Figure 1b). We have fully imaged ~0.65 km^2 of seafloor with >56,000 electronic still-images, with a coverage of >60% for the combined mosaic. Survey geometries and their characteristics are reported in Figure 2 and Table 1. This is the most extensive and complete image survey of an underwater hydrothermal vent field, and the resulting seafloor image mosaics are the largest of their kind to date.

[9] Owing to the lower image quality and characteristics of the Lustre'96 mosaic, this data set was not used in the digitization of active venting features. Individual images from this survey underwent a contrast-limited adaptive histogram equalization, and the original unequalized images are no longer available (see *Escartín et al.* [2008a] for details). The resulting mosaic is thus more difficult to interpret than those derived from OTUS imagery (2006, 2008, 2009 surveys), and here it is solely used to identify temporal variation in areas where active hydrothermal areas can be positively identified.

3.2. Image Processing and Mosaic Building

[10] Images were vertically acquired with an electronic still camera mounted on a deep-tow system or ROV and flown at an altitude of ~5–10 m from the seafloor. In all surveys, image acquisition was synchronized with strobe lights. The mosaic-building procedure is briefly summarized here and

Figure 1. (a) Bathymetric map of the Lucky Strike segment. Black box shows the location of Figures 1b, 1c, and 1d, the summit of the central volcano of Lucky Strike. (b) Bathymetric map zoomed and without any tracklines. Black line shows the contour of MoMARETO'06 bathymetic map box used for interpretation in Figures 5, 7, and 8; and red shaded area show emplacement of the AMC. (c) Navigation tracks for image surveys, acquired using the OTUS system mounted on ROV Victor 6000 (MoMARETO'06, MOMAR'08 and Bathyluck'09) and the ARGO II and TowCam deep-towed systems (Lustre'96 and Graviluck'06, respectively). The limits of the AMC are also indicated; the northern and southern terminations correspond to the limits of the seismic survey, and hence the AMC may extend further along-axis. (d) Navigation tracks of ROV VICTOR and HOV Nautile, with video imagery used to ground-truth the interpretation of the image mosaics. Bathymetry in Figures 1b, 1c, and 1d is from combined high-resolution seismics [*Combier*, 2007] and multibeam bathymetry [*Cannat et al.*, 1999; *Escartín et al.*, 2001].
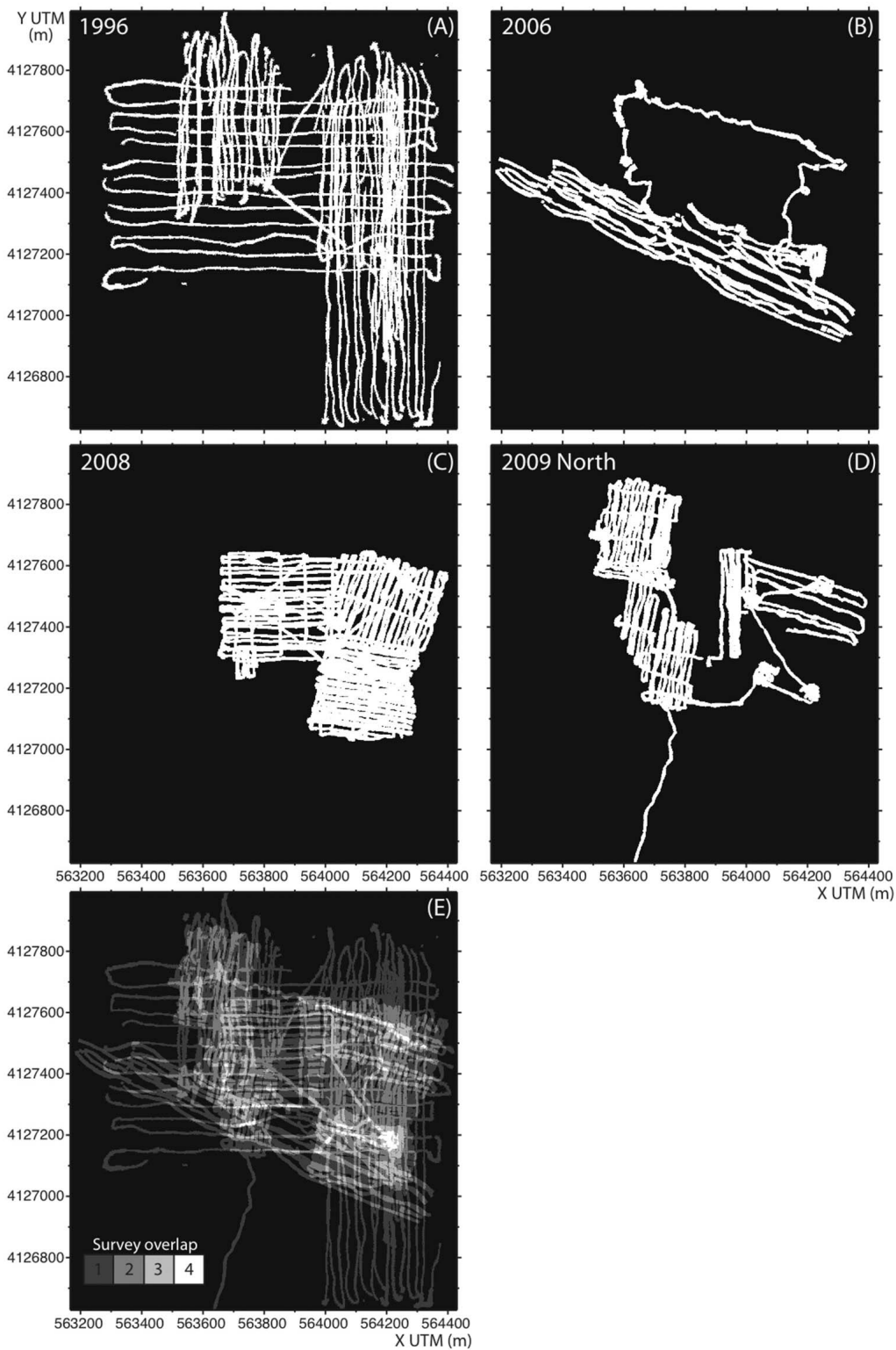
Figure 2. Maps showing the image mosaic coverage (white) for the electronic still image surveys at the Lucky Strike vent field for the (a) 1996, (b) 2006, (c) 2008, and (d) 2009 surveys. (e) The overall coverage and areas of overlap (tones of gray) are shown.

Table 1. Characteristics of Electronic Still Camera Image Surveys and Resulting Mosaics at the Lucky Strike Hydrothermal Field

Cruise	Year	Vehicle	Number of Photos	Surface[a] (m²)	Coverage[b] (%)	Hours of Survey	Resolution[c] (mm)
Lustre	1996	ARGOII	20283	388080	39	117	10
Momareto	2006	Victor	4626	149881	63	34	10
MoMAR	2008	Victor	21262	267179	80	101	10
Bathyluck	2009	Victor	10331	201592	72	33	5
Combined mosaic			56502	645339[d]	62	285	5, 10

[a]Surface of imaged seafloor by final seafloor image mosaics.

[b]Coverage: % of seafloor imaged by the mosaic imagery, within the surveyed area as delimited by the outline of survey tracks.

[c]The mosaic resolution corresponds to the pixel size in the final image.

[d]With repeated surveys, the reported surface corresponds to that of the final, combined mosaic, and does not include areas previously imaged (overlapping).

a full description and technical details are available elsewhere [*Prados et al.*, 2011]. First, acquired raw images are pre-processed to a) correct for uneven illumination from the lighting system and imaging geometry, b) equalize overall intensity among images, and c) correct the optical geometric distortion due to the camera lenses. This last correction requires a calibration to recover the intrinsic camera parameters, which was performed during the Bathyluck'09 cruise for the OTUS camera, and then used for the 2006, 2008 and 2009 mosaics, which were acquired with the same imaging system. Pre-processed images are scaled, rotated, and projected, to generate a navigation-based mosaic [*Escartín et al.*, 2008a] using vehicle navigation (location, altitude, heading, pitch and roll). Navigation was given by an USBL acoustic system, and location errors (~1–10 m depending on water depth and survey conditions) are orders of magnitude higher than the image (pixel) resolution (~1–10 mm). Image-based re-navigation of all surveys is therefore required. Matching of features from both consecutive and non-consecutive images is used to correct camera (vehicle) navigation. Feature matching and navigation corrections are iterated through an optimization. The final camera navigation trajectory allows the projection and geographical co-registration of images at the pixel level for all surveys. Image blending techniques are then applied to the mosaic to remove image edges and other mosaicing artifacts, and to insure that higher resolution imagery acquired closer to the seafloor is retained preferentially in areas with overlapping frames. This processing renders a seamless, single mosaic image [*Prados et al.*, 2011], with ~230,000 × 150,000 pixels at a resolution of 5 to 10 mm for the Lucky Strike data set (Table 1). Available near-bottom multibeam bathymetry (Momareto'06 cruise [*Ondréas et al.*, 2009]), which has a nominal horizontal resolution of 0.4 m and 1.5 m, provides information on seafloor morphology and tectonic structures (i.e., faults) that may be associated with hydrothermal discharge. As the navigation and processing of imagery and multibeam data were carried out independently, these data sets show relative offsets that are typically less than 10 m for well-known sites (e.g., Tour Eiffel, Montsegur, and Sintra).

3.3. Identification of Active Hydrothermal Outflow Zones

[11] Hydrothermal structures are clearly identifiable in the acquired seafloor imagery, and ground-truthed with in situ observations (e.g., video and still images from ROV or HOV dives, Figure 3). High temperature vents, with outflow temperatures of >200°C, are associated with plumes. Diffuse outflow at Lucky Strike is often associated with areas that contain white mats of philamentous bacteria in addition to macrofauna (e.g., mussels) (Figure 3a) [*Sarradin et al.*, 1999; *Desbruyères et al.*, 2001; *Martins et al.*, 2009], in association with anhydrite deposits, which have a white-mottled surface [e.g., *Langmuir et al.*, 1997; *Cuvelier et al.*, 2009]. Bacterial mats develop at temperatures <50°C [*Sarrazin et al.*, 2009], while anhydrate precipitates from seawater due to its retro-saturation when heated by hydrothermal fluids to temperatures of ≥100–150°C [*Bischoff and Seyfried*, 1978; *Møller*, 1988]; anhydrite deposits in contact with ambient-temperature seawater are re-dissolved [*Van Dover*, 2000]. Bacterial mats thus develop either in association with lower-temperature fluids (<50°C), or in the area of mixing of higher-temperature fluids and seawater. Consequently both the bacterial mats and anhydrite are reliable indicators of zones of hydrothermal outflow that are primarily diffuse with fluid temperatures as high as 150°C locally. Where bacterial mats are absent, hydrothermal deposits (anhydrite) are systematically
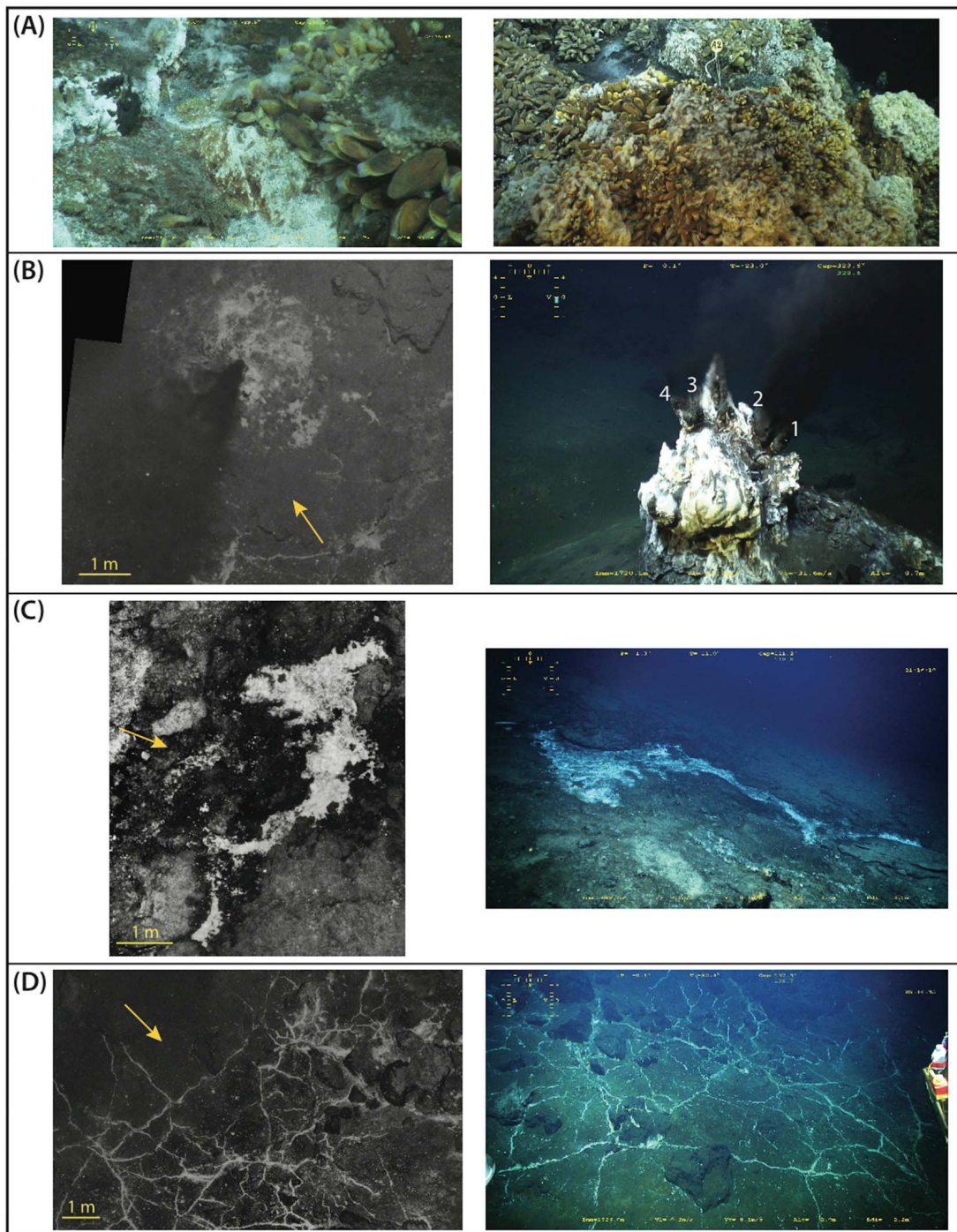
Figure 3. Photos and mosaic images of active diffuse outflow observed at Lucky Strike. (a) Two pictures showing bacterial mats, mussels and hydrothermal deposits associated to low-temperature diffuse venting. Examples of image mosaics (left) and corresponding oblique-view ROV imagery (right) of focused (Figure 3b) and diffuse venting (Figures 3c–3f), and of fossil outflow zones (Figures 3g and 3h). (b) South Crystal vent site, showing a hydrothermal mound with four high-temperature vents (numbers). (c) Patch of diffuse venting and associated bacterial mat. (d) Network of cracks at the Y3 site, at the base of a ~20-m high chimney. (e) North section of a hydrothermal mound at the Montsegur site. (f) Streaks of hydrothermal deposits remobilized downslope by gravitational processes. Numbers indicate matching features. The zone of diffuse active hydrothermal outflow is located under 2 (right image). (g and h) Dark seafloor patches interpreted as fossil outflow zones. Dashed line in the oblique view (right) corresponds to the limits mapped in the mosaic (left). Numbers indicate matching features at the oblique-view and mosaic images, and the arrows in the mosaic indicate the direction of the oblique view (Figures 3b–3h).
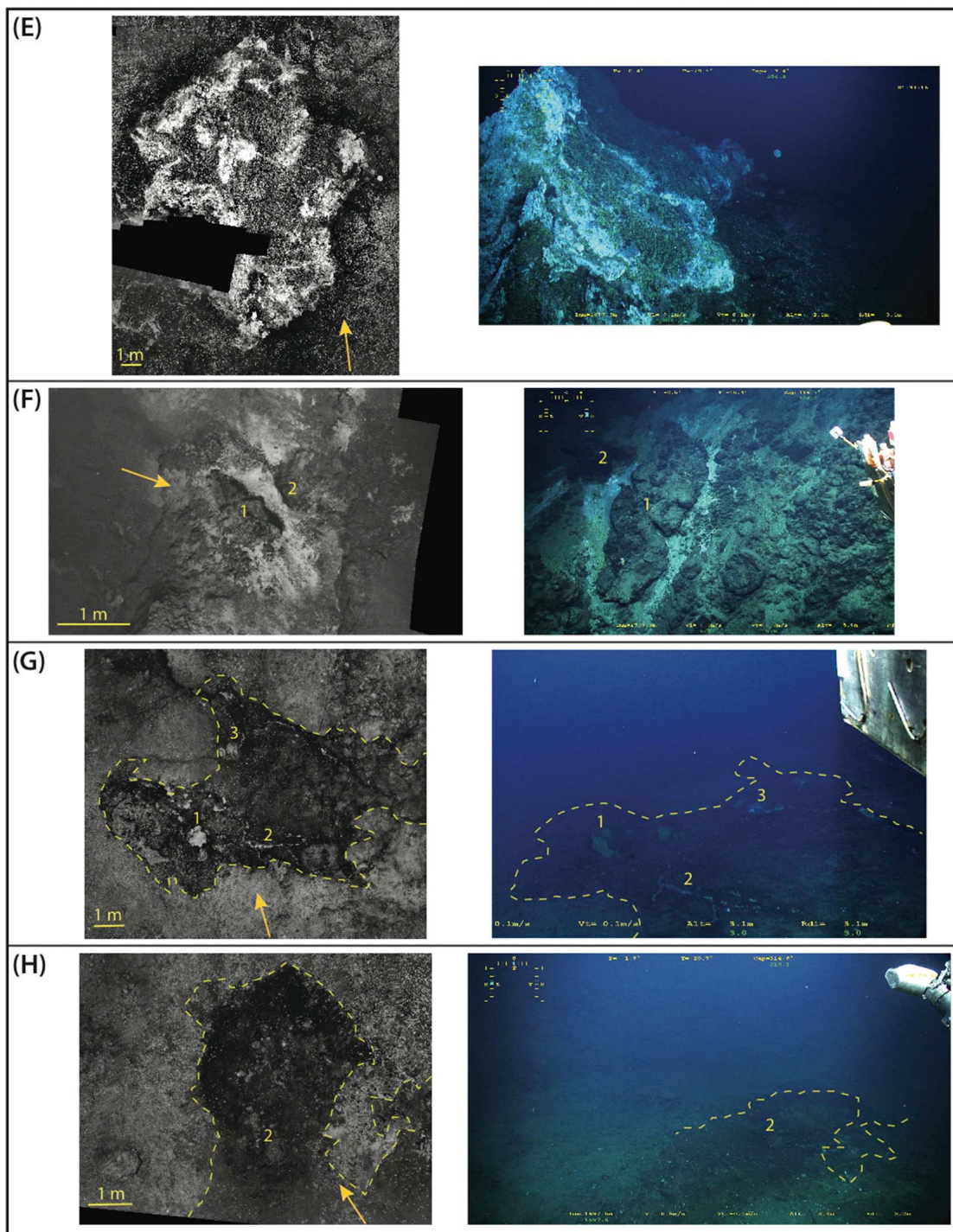
Figure 3.   (continued)

associated with focused high temperature sources, and therefore indicate recent or active outflow.

[12]   Actively venting areas can thus be readily identified through visual inspection of image mosaics and associated oblique-view imagery. Using dedicated image-viewing software (see *Escartín et al.* [2008a] for details), we digitized the limits of individual features, based on the full-resolution mosaic scenes (areas ~10 m wide, with a pixel resolution of

Table 2. List of Active, High-Temperature Hydrothermal Sites at Lucky Strike, With Their Position and Depth, Identified From Mosaic Images and ROV Observations[a]

Sites	Xutm (m)	Yutm (m)	Lon. (W)	Lat. (N)	Depth (m)	Matching
SE						
Montsegur[b]	564214	4127075	32° 16.534′	37° 17.284′	1701	U.S.4/U.S.6?
U.S.4?	564217	4127064	32° 16.532′	37° 17.278′	1700[c]	vent 2607?
U.S.6?	564186	4127071	32° 16.553′	37° 17.282′	1703[c]	
U.S.7?	564186	4127079	32° 16.553′	37° 17.286′	1700[c]	Cimendef?
Tour Eiffel[b]	564216	4127184	32° 16.532′	37° 17.343′	1684	
Aisics[b]	564219	4127176	32° 16.530′	37° 17.338′	1689.3	
Isabel[b]	564059	4127247	32° 16.638′	37° 17.377′	1683.7	
P.Chimiste?	564069	4127274	32° 16.631′	37° 17.392′	1648[c]	
PP4?	564124	4127349	32° 16.593′	37° 17.432′	1665	
X10[b]	564059	4127193	32° 16.638′	37° 17.348′	1700[d]	PPS?
X3[b]	564233	4127074	32° 16.521′	37° 17.283′	1700[d]	
NNE						
Y3[b]	564008	4127495	32° 16.671′	37° 17.512′	1727.3	
Sintra[b]	564263	4127529	32° 16.498′	37° 17.529′	1614.7	
St. Liberty[c]	-	-	32° 16.470′	37° 17.560′	1628	
St. Liberty[e]	-	-	32° 16.490′	37° 17.590′	1646	
SW						
White Castle[b]	563717	4127255	32° 16.869′	37° 17.383′	1708.9	
Crystal[b]	563640	4127384	32° 16.921′	37° 17.453′	1723.3	
S. Crystal[b]	563619	4127368	32° 16.935′	37° 17.445′	1720.5	
Pico (mosaic)?	563722	4127277	32° 16.866′	37° 17.395′	1725	
Pico (ROV)[b]	563651	4127395	32° 16.913′	37° 17.459′	1725	
Cypres[b]	563725	4127379	32° 16.863′	37° 17.450′	1738.7	
Snowman[b]	563625	4127383	32° 16.931′	37° 17.453′	1722	
Nuno?	563621	4127460	32° 16.933′	37° 17.494′	1727[c]	
Helene?	563687	4127469	32° 16.888′	37° 17.499′	1722[c]	
Sapins[b]	563614	4127359	32° 16.938′	37° 17.439′	1718.6	
NW						
Bairro Alto?	N/A	N/A	N/A	N/A	N/A	Elisabeth/Jason?
Jason?	563615	4127723	32° 16.936′	37° 17.637′	-	Elisabeth/B.A?
Elisabeth?	563643	4127743	32° 16.917′	37° 17.647′	-	Jason/B.A?

[a]The correspondence to other site names in the literature is also provided. Uncertainty in naming correspondences is indicated by question marks.
[b]This study.
[c]As reported by *Charlou et al.* [2000].
[d]Depth of Montsegur and nearby sites.
[e]As reported by *Langmuir et al.* [1997].

5–10 mm), as described below. Close inspection of the data have allowed us to identify active and fossil high temperature vents, and four types of diffuse outflow at Lucky Strike, likely associated with different flow regimes, and these have been digitized separately. For the purpose of this digitization, we primarily use the 2008 mosaic, which provides the most complete coverage of the field. The remaining mosaics complement the interpretation at gaps and unmapped areas (Figures 1b and 2).

[13] In addition to hydrothermal deposits and bacterial mats, the imagery reveals other white areas that are not related to hydrothermal activity. These include sediments with a white appearance in the black-and white imagery, overexposed frames due to image acquisition at close range, or shell chaff on seafloor, primarily in the vicinity of actively venting sites. These features are readily distinguishable

from the active hydrothermal areas, and are therefore not included in the interpretation. Features that we could not positively identify as hydrothermal were not digitized.

3.3.1. Active High-Temperature Vents and Chimneys

[14] High-temperature fluids venting at chimneys and hydrothermal mounds are easily recognizable visually in oblique-view imagery (ROV or submersible) owing to their morphology and size, and the presence of plumes in the water column (Figure 3b). Their identification is more difficult in vertical-view imagery, owing to their sub-vertical structure and small footprint (Figure 3b), even if the main venting areas are well known [*Langmuir et al.*, 1997; *Humphris et al.*, 2002; *Ondréas et al.*, 2009]. Vent locations are determined primarily in

Table 3. Summary of Distribution of Hydrothermal Outflow Types Identified at Lucky Strike, Including the Number of Structures Identified, Mapped Surface, and Relative Proportions for the Site, for the Three Different Substrate Types Defined at Lucky Strike

	Number of Structures	Total Surface (m^2)	Diffuse Outflow Type (%)	S1 (%)	S2 (%)	S3, W/E[a] (%)
Patch	4742	975	55	41	72	76.5/79
Cracks	687	143.5	8	9	6	6.5/11
Mounds	36	630	36	50	21.5	16.9/0
Streaks[b]	247	*20.25*	1	0	<0.5	0.1/10
Active Vents	67	-	-	55	3	9/0

[a]Relative importance of diffuse hydrothermal outflow types vary significantly between the W and E fault scarps, and are therefore reported separately here.

[b]The surface of active venting associated with streaks is estimated to 5% of the digitized area, as these correspond primarily to gravity-driven remobilization of hydrothermal deposits (see text for details).

ROV video imagery coupled with its navigation (more than 1000 h of video available from MoMAR'08, Bathyluck'09, MoMARSAT'10 and '11 cruises; see tracks in Figure 1c), in addition to matching features in the mosaics images (Figure 3b), as well as the correspondence to sites reported in the literature (Table 2).

3.3.2. Types of Diffuse Outflow

[15] Image mosaics reveal four types of diffuse outflow (Figure 3): flow through irregular, continuous seafloor areas (referred to as *patches from here on*); through well-defined fractures (*cracks*); through the flanks of hydrothermal constructions (*mounds*); and flow indicated by streaks of hydrothermal minerals mobilized down steep slopes from the sources (*streaks*). These diffuse outflow types often show a continuum between them, with gradual transitions and complex associations.

[16] Individual digitized features are assigned to one of the four diffuse outflow types, allowing us to quantify the abundance and distribution of actively venting areas throughout the field. Large features are digitized as polygons, from which we can estimate the area of active hydrothermal outflow. Small features with average diameters of less than ~0.20 m are arbitrarily digitized as single points, and assigned a surface area of 0.01 m^2, corresponding to the average size of a representative sample of such features digitized throughout the study area. These small patches are a minor fraction of the total surface area of active diffuse outflow, and hence inherent errors in surface calculations are negligible. Overall, the surface area calculated here is likely a minimum estimate, first due to the partial seafloor imaging (62%). Even if image surveys locally had 100% coverage at active sites (see Figure 2e), some active areas may have not been imaged or identified. Second, additional hydrothermal activity may be present beyond the surveyed areas (Figure 1). Systematic searches and transits in successive cruises have yielded no additional active vents (see Figure 1d), suggesting that the extent of active venting at the Lucky Strike field is well-defined.

[17] *Patches*. We define patches as irregular, discrete areas of the seafloor that display a more or less continuous white surface throughout, with no apparent hydrothermally constructed feature associated (Figures 3c). Their size is highly variable, and can range from a diameter of a few centimeters (limit of the mosaic resolution) to tens meters in a few instances. In situ ROV observations indicate that these correspond to either diffuse fluid discharge through a porous surface, or to areas conductively heated from below. Individual patches can exceed 20 m^2, with a typical area of ~0.5 m^2.

[18] *Cracks*. Hydrothermal fluids may outflow along individual fissures or networks of fractures, around which bacterial mats and hydrothermal deposits concentrate (Figure 3d). As in the case of patches, we digitize the edges of individual cracks and associated mats and deposits when they are sufficiently wide (>10 cm). Networks of narrow cracks preclude this analysis (e.g., Figure 3d), and are instead digitized as lines with lengths varying from centimeters to meters. We have carried out systematic measurements within a crack network at both the Y3 site (this study) and the Tour Eiffel site [*Mittelstaedt et al.*, 2012], yielding in both cases an average crack width of ~4 cm, a value used to estimate the surface area associated with these narrow cracks. In situ temperature measurements and close-up video imagery show convective outflow that varies significantly along individual fractures, with measured fluid temperatures ranging from <20 to ~100°C over distances of <10 m along a single crack.

[19] *Mounds*. Several sites are characterized by broad sulfide mounds, with base diameters ranging from 1 m to 20 m, and an elevation of up to several meters above surrounding seafloor (e.g., Figure 3e). At Lucky Strike, these structures display diffuse venting across their flanks, which are extensively covered by bacterial mats and hydrothermal deposits, and often colonized by macrofauna (e.g., mussels).

In extreme cases of fluid flow localization, such as the Y3 hydrothermal vent, outflow is focused along a single chimney several to tens of m high, with limited diffuse outflow on its walls; these structures are identified as high-temperature vents (See section 3.3.1) and not as mounds.

[20] *Streaks.* In areas of steep topography such as fault scarps and the flanks of major hydrothermal deposits, we find white streaks up to several meters in length and a few tens of centimeters in width (Figure 3f), elongate downslope, and emplaced on talus (Figure 3f, right). Video observations indicate that these structures originate upslope at cracks with active, diffuse venting, and that they are not associated with philamentous bacteria and other hydrothermal fauna (e.g., mussels). This morphology and geometry indicates a gravity-driven downslope remobilization of hydrothermal deposits, probably anhydrite. Unlike the three other diffuse outflow types described above, the digitized surface does not correspond to actively venting area, but to that of hydrothermal materials remobilized from its source. From systematic video observations we estimate that the fraction of active diffuse outflow along a streak feature is very small (5% or less) relative to the total digitized area (see examples in Figure S1 in the auxiliary material).[1] To correct this bias, values of the surface area of active venting reported in Table 3 are corrected accordingly.

3.4. Temporal Variability in Active Venting From Image Mosaics

[21] The Lustre (1996), Momareto (2006), Gravyluck (2006), MoMAR (2008) and Bathyluck (2009) mosaics provide overlapping coverage of the seafloor at the Lucky Strike hydrothermal field (Figures 2a–2d) over more than 40% of the surveyed seafloor. This overlap occurs primarily at or around active hydrothermal sites (Figure 2e). Image mosaics can thus be used to identify variations in the size, nature, and/or distribution of hydrothermal activity as described above, at time-scales that vary between 1 year (2008–2009 surveys) and 13 years (1996–2009). In addition, we can determine if temporal changes are local or occur at a field-scale. Figure 4 shows examples from four active sites, displaying an overall reduction or increase in their size, changes in their continuity and intensity, or the appearance or disappearance of active areas. Differences in image quality between different surveys

(e.g., imaging conditions, resolution of original images) preclude a quantitative evaluation of these changes, and hence observations reported here are qualitative. A systematic inspection of all the image mosaics allowed us to identify 100 active sites with overlapping imagery distributed throughout the Lucky Strike hydrothermal field.

3.5. Fossil Hydrothermal Outflow

[22] Processed image mosaics reveal distinctly dark seafloor areas (Figures 3g and 3h) with sharp limits against surrounding sedimented terrain of a lighter tone, which are particularly visible in zones of seafloor with low relief associated with the 'hydrothermal slab' substrate (e.g., SE of the survey area). These structures are not identified in steep terrain such as fault scarps and flanks of massive hydrothermal deposits, likely owing to the relief, changes of lightning, and the heterogeneous and discontinuous nature of the seafloor texture. ROV and HOV observations demonstrate that numerous inactive and active hydrothermal structures are found within. Numerous inactive chimneys, both standing and fallen, testify for a history of focused, high-temperature venting. Traces of fossil diffuse outflow are more difficult to identify, but the presence of yellow bulbous hydrothermal constructs several 10s of cm in height, often lined up along fractures, indicate prior diffuse activity. No samples to determine the composition and origin of this yellow material exist, but their morphology and association with fissures suggest that they originated from precipitation at outflow along cracks (Figures 3g and 3h). Submersible observations demonstrate that the dark areas correspond to a superficial patina covering the seafloor, which has not been sampled to date ascertain its nature. We propose that the dark areas may correspond to hydrothermal precipitates (oxides) from diffuse outflow through the seafloor, from hydrothermal fallout from nearby vents, or a combination of both, owing to the clear association with fossil venting structures.

[23] Available microbathymetry also reveals hydrothermal deposits E and NE of the lava lake, described in detail by *Ondréas et al.* [2009], and corresponding to the hydrothermal deposit substrate defined below. Here individual conical hills up to 15 m in height and 25 m in diameter composed of sulfide blocks and hydrothermal rubble, likely pinpoint extinct hydrothermal sites of a similar size to that of the present-day Tour Eiffel site. The summits of these structures, clearly identifiable in the bathymetry (Figure 5), are used to

---

Figure 4. Examples of temporal variability documented by repeated image surveys and for selected sites; locations are given in UTM (m): Site 1: X = 564082, Y = 4127223; Site 2: X = 564022, Y = 4127493; Site 3: X = 564080, Y = 4127183; Site 4: X = 564067, Y = 4127206. Numbers indicate matching features and red arrows indicate temporal changes.
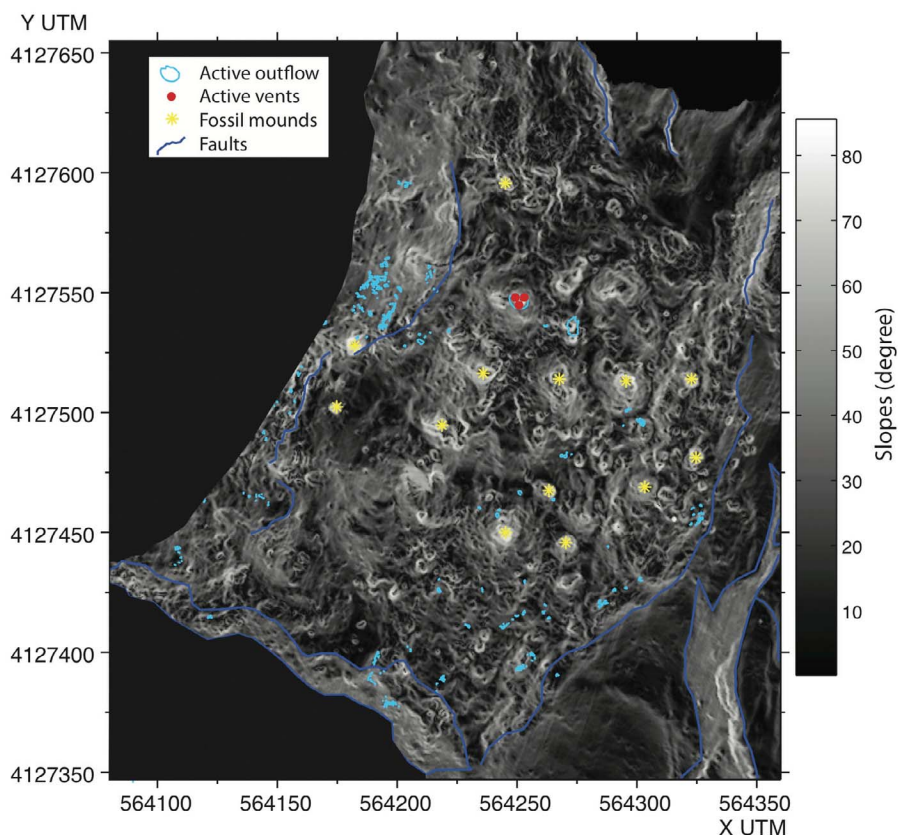
Figure 5. Slope map derived from multibeam bathymetry [*Ondréas et al.*, 2009], showing the interpreted summit of fossil hydrothermal mounds (yellow), as well as active diffuse outflow and vents digitized from the image mosaics.

complement the map of fossil structures identified in the image mosaics (Figures 6 and 7).

3.6. Nature of Substrate and Fault Identification

[24] Substrate nature, which varies throughout the Lucky Strike area, may play a role in the geometry and nature of hydrothermal discharge. We have defined three substrate types, based on their morpho-tectonic character, on prior geological and geophysical studies in the area [*Humphris et al.*, 2002; *Ondréas et al.*, 1997, 2009], and in situ ROV observations (this study, Figures 1d and 3). The first type of substrate corresponds to the "hydrothermal slab (i.e., a cap of hydrothermally cemented breccia [*Langmuir et al.*, 1997; *Ondréas et al.*, 1997, 2009]). Slab is identified in relatively smooth seafloor that is cross-cut by normal faults with small vertical relief (typically 10 m or less), readily recognizable in the bathymetry data (previously identified as H3 by *Ondréas et al.* [2009]). This substrate, which is found at the E and S of the lava

lake (S1 in Figure 7), hosts several hydrothermally active areas with associated hydrothermal deposits (see image mosaic example in Figure 6), as well as dark areas interpreted as fossil outflow zones. The second substrate type corresponds to laterally continuous, massive hydrothermal deposits located E of the lava lake and the bounding fault scarp (S2 in Figure 7; referred to as H2 by *Ondréas et al.* [2009]). S2 deposits extend ~300 m along-axis, and ~200 m across it, corresponding to rugged terrain, and composed of several mounds 10–20 m high with slopes of >30° (Figure 5). The third substrate (S3 in Figure 7) corresponds to the slopes of the major axial graben-bounding fault scarps, identified E and W of the lava lake (graben bounding faults). The scarps, ~100 m in vertical relief and sloping >30°, display a complex morphology with talus, blocks, and rubble. In plan view, this substrate covers ~550 m along-axis and has a variable width, with a maximum of 350 m on the W fault scarp. The top of the E fault scarp is ill-defined, as it transitions to the hydrothermal deposits to the East (S2). While hydrothermal activity is found within these fault scarps, the associated deposits are not
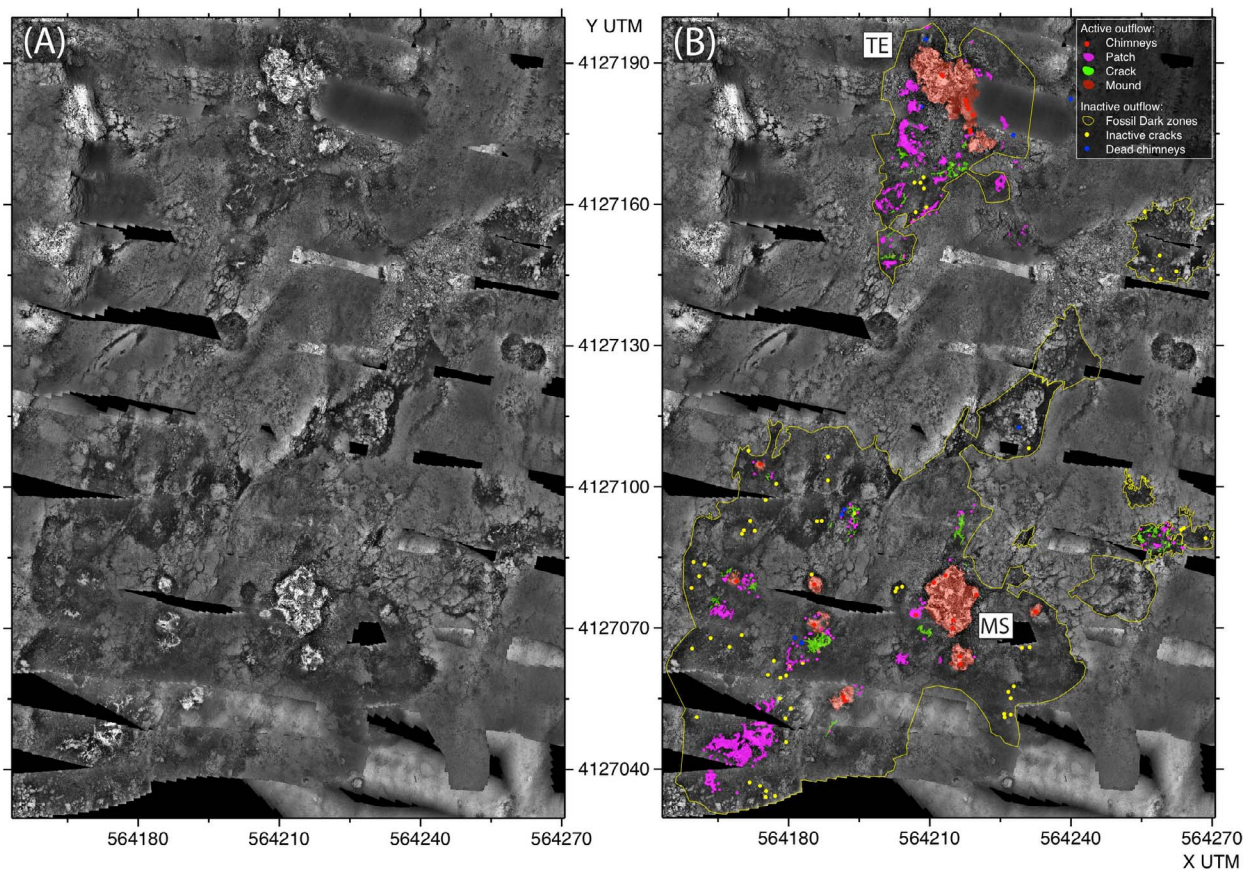
Figure 6. (a and b) Detail of the image mosaic of the southeastern part of Lucky Strike hydrothermal field (Figure 6a) and identified hydrothermal features (Figure 6b), both active and inactive, obtained from image mosaic interpretation and in situ observations. Note that all the active focused and diffuse hydrothermal discharge is located within the areas interpreted as fossil outflow (dark seafloor). The seafloor imagery is the 2008 mosaic complemented in the background by the 2006 and 2009 mosaics to reduce imaging gaps. Axes correspond to UTM coordinates in meters. Names of sites: MS: Montsegur, TE: Tour Eiffel. Note that round dark areas not digitized correspond to feature made by the Nautile submarine ballast, thus aren't from hydrothermal origin.

continuous, likely due to gravitational collapse over the history of hydrothermal activity. Individual fault scarps are identified and digitized from multibeam bathymetry [*Ondréas et al.*, 2009] (Figures 5, 7 and 8a). In addition to the fault substrate (S3), we digitized well-defined upper and lower scarp limits for the larger faults (vertical throws of 5 m or more). Smaller faults with throws of <5 m, are digitized as single lines through the center of the scarp (Figure 7 and 8a).

4. Results

4.1. Distribution and Nature of Hydrothermal Outflow

[25] The image mosaics of the Lucky Strike hydrothermal field document activity over an area

900 m across-axis and ∼600 m along it (Figures 1 and 2). As described in prior studies, active sites surround the central depression ('lava lake') [e.g., *Langmuir et al.*, 1997; *Humphris et al.*, 2002; *Ondréas et al.*, 2009], but are absent from its interior (Figure 7). Systematic optical mapping of the field demonstrates that diffuse outflow, corresponding to <0.5% or the surveyed seafloor surface (∼0.65 km^2; Table 1), occurs over an area larger than that defined by known high-temperature vents [e.g., *Humphris et al.*, 2002; *Ondréas et al.*, 2009]. The distribution and relative abundance of diffuse outflow types is highly variable (Figure 7), both at the scale of a single site and among different sites. The dominant outflow types are patches and mounds, corresponding to 55% and 36% of the surface of active diffuse outflow (Table 3). Individual mounds can cover large areas
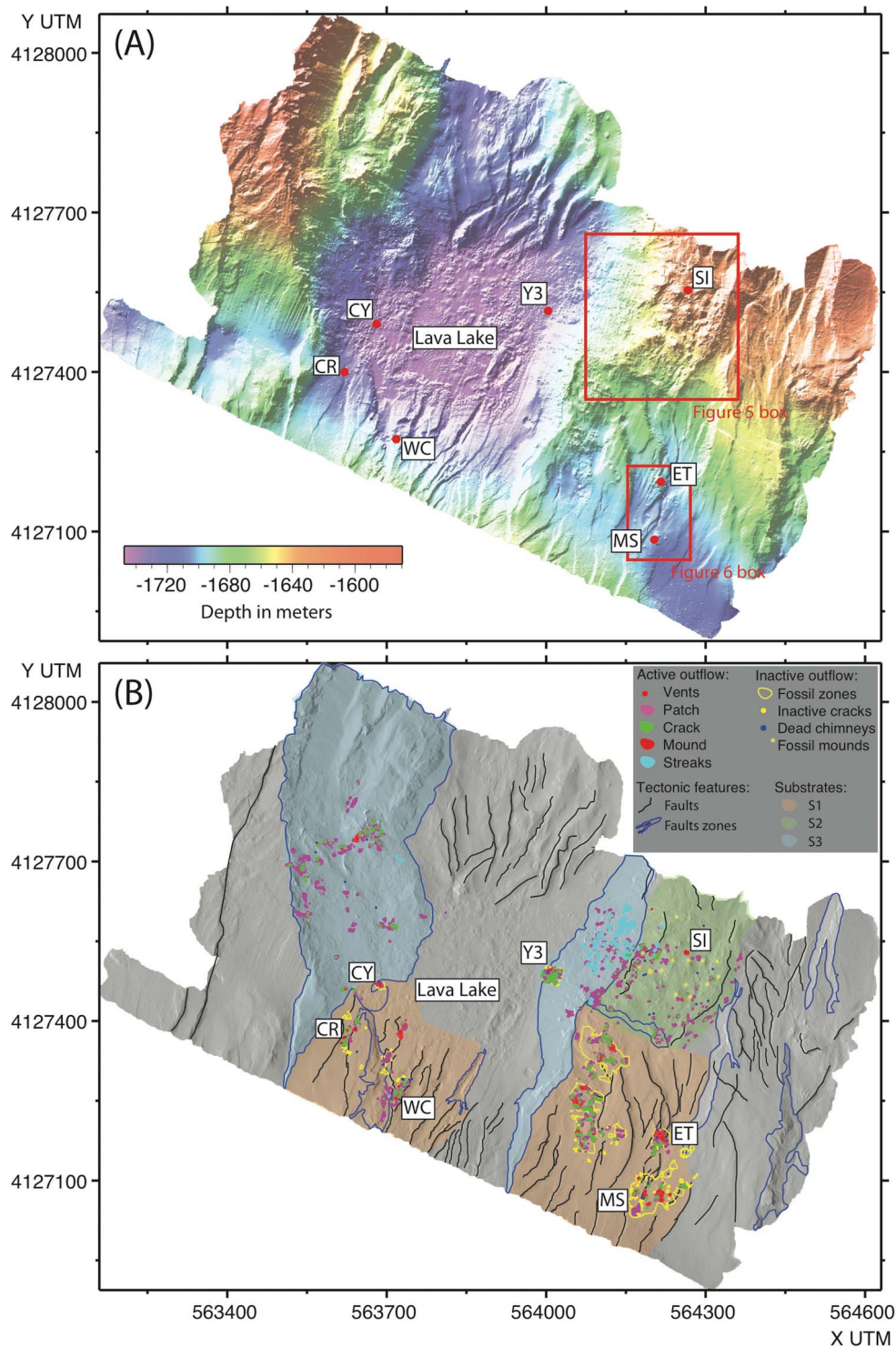
Figure 7. (a) High-resolution bathymetry map, from the MoMARETO'06 cruise (see *Ondréas et al.* [2009] for details), gridded at 0.5 m. (b) Map showing all identified active and inactive hydrothermal features from the Lucky Strike field, the substrates as defined in the text, and the fault scarps found in the study area. The map extend corresponds to the 2006 MoMARETO bathymetry survey, which covers all the known areas of active venting of the Lucky Strike field. Substrates: S1: cap of hydrothermally cemented breccia, referred to as 'slab' in the text. S2: laterally continuous, massive hydrothermal deposits forming a rugged terrain. S3: slopes of the major axial graben-bounding fault scarps displaying a complex morphology with gravity collapses, as blocks and rubble, associated with talus. Names of sites: CR: Crystal, CY: Cypres, IS: Isabel, MS: Montsegur, SI: Sintra, TE: Tour Eiffel, Y3: Y3.
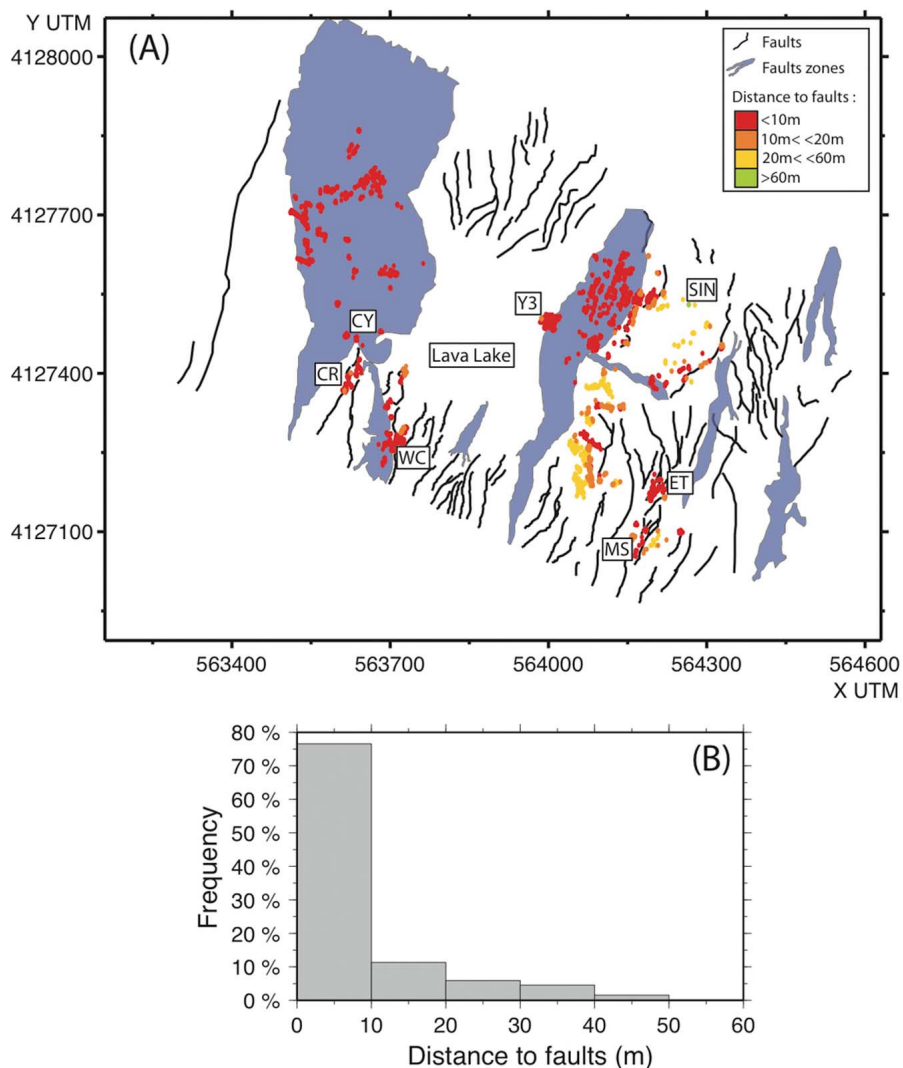
Figure 8. (a) Map showing the distribution of active venting areas (diffuse) and faults identified from microbathymetry. (b) The corresponding histogram of distance to the closest fault for each active feature identified. Note that >75% of the features are within less than 10 m from fault scarps, and only 5% of them are at distance >20 m. The latter are concentrated over the hydrothermal substrate that likely masks underlying faults dissecting the basement. Names of sites are the same as ones given in Figure 7.

(e.g., 107 m² and 134 m² at the Montsegur and Tour Eiffel sites, respectively), and hence a relatively low number of these structures account for a sizable proportion of the documented diffuse flow.

[26] There is a link between substrate type and the observed style of diffuse outflow (Figure 7), indicating that the permeability structure of the shallow crust plays a role on the nature of discharge at this field. The relatively flat seafloor morphology of the 'slab' substrate in the southern part of the study area (substrate S1, Figure 7) more clearly shows the organization of diffuse outflow, due to the lack of

complex topography. Here, we observe diffuse flow associated with high-temperature venting in well-defined clusters that are separated by seafloor showing no active hydrothermal discharge. This area also has the highest concentration of both the identified high-temperature vents (55 out of 67 vents) and the zones of diffuse outflow (∼1090 m² and 62% of the surface of mapped structures, see Table 3). The surface area of diffuse outflow is dominated by the presence of large mounds (∼50%) surrounded by patches (∼40%), while zones with actively venting cracks account for <10% of the active area of diffuse outflow.
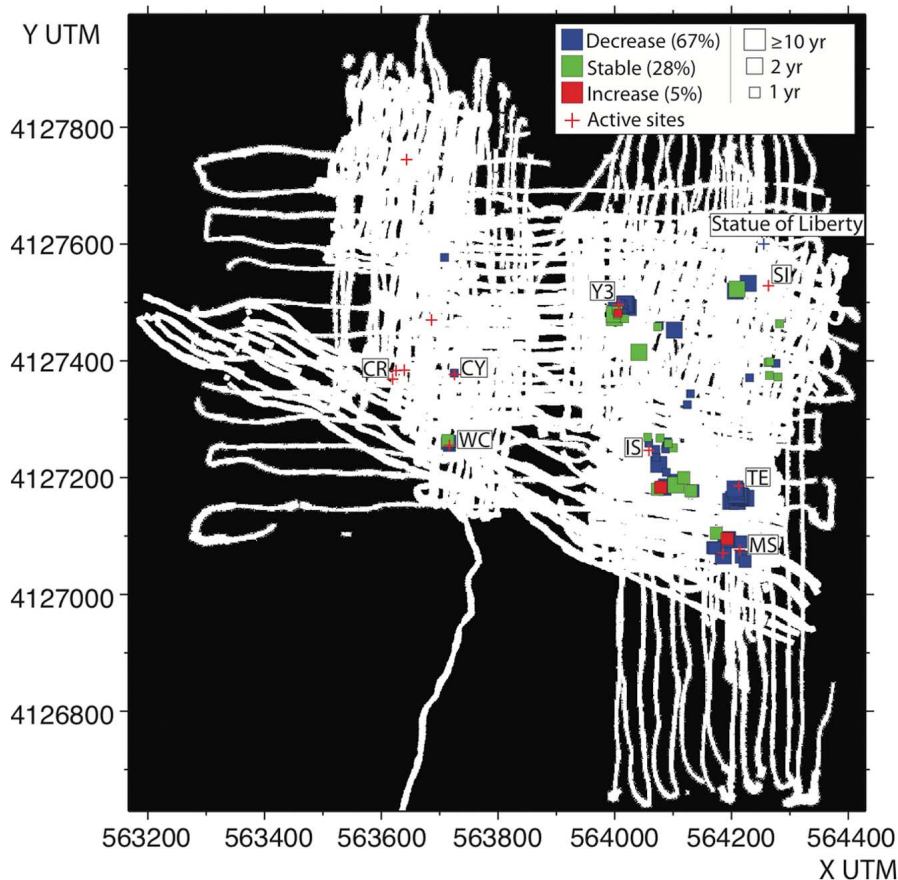
Figure 9. Temporal evolution of diffuse hydrothermal activity at the Lucky Strike site based on the comparison of mosaics at overlapping areas (1996–2009) and from limited in situ observations (1993–2009) at the Statue of Liberty site (now extinct). Note that changes are documented at time-scales varying between 1 and 13 years, denoted by the size of the symbols.

[27] The nature of discharge and its abundance through the hydrothermal substrate (S2, Figure 7) and on major fault scarps (S3) are different from that hosted by the slab substrate. The hydrothermal substrate (S2) is characterized by coalescing fossil hydrothermal edifices [*Ondréas et al.*, 2009], primarily hosting patches of diffuse outflow (~70% of S2 active surface), while active high temperature vents are scarce (3 vents concentrated at the Sintra site, out of a total of 67 for the whole field). Outflow along the fault scarps (S3) differs between the E and W scarps flanking the lava lake. The E scarp, which is the steepest, lacks mounds but displays streaks of hydrothermal deposits remobilized downslope (10% of active surface). In contrast, the W scarp is less steep, lacks streaks, and hosts two active hydrothermal mounds. Outflow through patches dominates the diffuse outflow on the fault scarps. High-temperature vents are documented at the Y3 site on the E flank and the Helene and Barrio Alto sites on the W flank, although additional, unmapped high-temperature vent sites may exist, particularly on the W fault scarp. The distribution of hydrothermal activity is unequal among the sites. Substrates S1, S2 and S3 host 63%, 10%, and 27% of the active diffuse venting surface area documented at the Lucky Strike hydrothermal field and account for 0.6%, ~0.3% and 0.2% respectively of the total surface.

[28] The detailed image mosaic interpretation reveals variability in the structure of hydrothermal outflow among individual sites. For example, the Y3 hydrothermal site is dominated by a 20-m high chimney with numerous vents at the summit. Around the Y3 chimney, diffuse outflow principally occurs at patches, but is also observed across an extended crack network adjacent to this chimney (72% patches, 28% cracks; Figure 3d). In contrast, at the Tour Eiffel and Montsegur sites (Figure 6),

hosted in the slab substrate, outflow is dominated by active hydrothermal mounds (72% and 92% of the mapped diffuse outflow surface area, at each site respectively), with outflow through patches differing significantly between the two sites (23% and 4% respectively; Figures 3 and 6). These inter-site variations demonstrate that heat flux estimates cannot be reliably extrapolated from individual sites to the entire hydrothermal vent field.

[29] To investigate the relationship between digitized faults and active vents in our study area, we calculate the distance from outflow zones to the nearest mapped faults (Figure 8). For hydrothermal zones within the scarps of larger faults (e.g., substrate S3, or the larger faults, Figure 8a), we assign a distance of 0 m. We observe that >75% of the active sites occur within 10 m of a fault scarp (Figure 8b), with an average distance of ~7 m, and hence within the error in of geographic registration between multibeam bathymetry and image mosaics (~10 m). Sites hosted in substrate S2 (Figure 7) may show a bias toward longer distances. Here, the hydrothermal deposits likely cover normal faults dissecting the basaltic basement that serve as present-day and paleo-conduits for the active and inactive vents in the area. However, these sites represent a small fraction (~10%) of the total active sites identified.

4.2. Temporal Variability From Repeated Image Mosaics and in Situ Observations: 1–20 Years Time Scales

[30] Systematic examination of mosaics reveals 100 locations with active venting and overlapping imagery, encompassing the four types of diffuse outflow described (Figures 4 and 9). Comparisons among mosaics at these sites, summarized in Figure 9, indicate a systematic decrease in activity at 67 of the 100 sites, while only 5 sites show an apparent increase, and the remaining are stable. This pattern is consistent at all time-scales investigated, from 1 year (2008–2009 mosaics) to 13 years (1996–2009), although the number of observations for the longer time scale is reduced owing to the image quality of the Lustre'96 mosaics (Figure 4). Despite this overall diffuse venting decrease, the location and general structure of the hydrothermal outflow remained stable over the 1996–2009 time period. Furthermore, we observed no development of new outflow zones or the full disappearance of those existing.

[31] In addition to direct observation of changes in diffuse outflow from mosaics, circumstantial evidence of temporal change exists from submersible and ROV observations. For example, the Statue of Liberty site was active at the time of its discovery in 1993 [*Langmuir et al.*, 1997], but subsequent observations 26 years later (ROV VICTOR Dive #389, Bathyluck'09 cruise report) demonstrate that this site is now inactive. An overall decline was also observed during dives between 2008 and 2010 at hydrothermal sites at the base of the western fault scarp. Here hydrothermal mounds with extensive diffuse outflow show a clear decrease of the continuity and intensity of bacterial mats on vertical walls. Hence, while these observations cannot be validated with the existing mosaics at individual sites (i.e., at Statue of Liberty), they indicate an overall pattern of decline which is consistent with in situ observations from ROV and HOV dives to the Lucky Strike hydrothermal field during the last two decades.

4.3. Temporal Variability From Mosaic Interpretation and Multibeam Bathymetry: Long Time Scales

[32] In areas with 'slab' substrate (S1, Figure 7), the processed image mosaics reveal the distinct dark zones with well-defined edges (Figures 3g, 3h and 6), described in detail in section 3.5, that we interpret as zones of fossil hydrothermal discharge. These structures thus record a change in the size of discharge zones at Lucky Strike, but not in their spatial distribution, as indicated by their systematic association with active venting.

[33] Outside the hydrothermal slab substrate, such dark features are not observed. The substrate associated with both the hydrothermal deposits and the fault scarps (S2 and S3, Figure 7), display a locally rugged terrain, as well as steeper slopes (e.g., flanks of hydrothermal mounds and the sloping fault scarps and associated talus). With such complex topographies relative to the smooth and slightly sedimented slab terrain, evidence of past hydrothermal activity may have not been preserved in these areas (e.g., mass wasting and gravity movements), or may not be readily identifiable due to relief and illumination conditions.

[34] Another source of evidence for long-term variability in the activity of the field comes from seafloor observations and multibeam bathymetry from substrate S2 (Figures 5 and 7). This area hosts more than 10 fossil hydrothermal structures (i.e., piled blocks of sulfides) with a size and height similar to those of the Tour Eiffel site. The only active structure at the present time is Sintra,

which shows a weak discharge with relatively low outflow temperatures (207°C in 2009), and no venting at higher temperatures. The Statue of Liberty site, active in 1993 is now extinct, and the rest of the hydrothermal piles do not show any signs of recent activity. Furthermore, diffuse outflow throughout S2 is restricted to only a small fraction of the seafloor (Figures 5 and 7). The presence of several hydrothermal mounds closely associated spatially is thus consistent with enhanced discharge in the past, at least relative to the present-day observed activity.

5. Discussion

5.1. Surface Distribution of Hydrothermal Discharge and Its Plumbing System

[35] The spatial distribution and structure of hydrothermal outflow at the seafloor may be used as a proxy for the subseafloor geometry of fluid discharge. Numerical models suggest that, for uniform crustal permeabilities, upwelling of hydrothermal fluids is organized in a discrete plume with a discharge zone at the seafloor that has a footprint of a few hundred meters in diameter [*Fontaine et al.*, 2008]. This spatial scale is similar to that of the entire Lucky Strike hydrothermal field, and much larger than the typical size of individual sites observed within it (from a few m to tens of m in diameter). This disparity in spatial scales may be explained by a hydrothermal discharge originating from a single upwelling zone at depth, and that it is re-organized and split in the shallow crust along smaller upwelling zones, which would directly feed the discharge zones identified at the seafloor (Figures 6 and 7).

[36] Maps in Figure 10 show the distance to the nearest active hydrothermal feature, and reveal the overall spatial organization of the hydrothermal discharge. This distribution is similar for both focused and diffuse venting (Figures 10a and 10b respectively). Differences in structure are restricted to the NE, where Sintra is the single site with focused, high-temperature venting and where the rest of the activity is diffuse (Figure 10b). At the level of the Lucky Strike field there is a clear split of the hydrothermal outflow into two zones, E and W, which correspond to the faults flanking the axial graben dissecting the central volcano. At smaller spatial scales, and within each of the graben flanks, the distribution of hydrothermal features reveals different levels of clustering. Using the distribution of sites (Figure 7) and distance maps (Figures 10a

and 10b), we identify twelve main clusters based primarily on the focused flow sites (Figure 10a, black dashed lines, also reported in Figure 10b for comparison diffuse flow structure). The overall agreement in the structure of both focused and diffuse outflow suggests that both modes of discharge are closely related, reflecting mixing between cold seawater and upwelling high-temperature fluids within the upper crust.

[37] We propose that outflow distribution at the seafloor and the clustering of sites reflect, to a first order, the plumbing system underlying this hydrothermal field, in terms of geometry, branching paths of the upflow, and its depth. We use a k-means clustering technique based on the Euclidian position and relative distance between all features as defined by their centroid position, and determined from the digitized geometry of individual features. Clusters are hierarchically related, based on their relative mean distances (between cluster centroids). Figure 10c shows the structure for 12 clusters, which corresponds to the number of outflow zones defined visually in Figure 10a. Assuming that the clustering distance (horizontal) is a proxy for depth (vertical distance), we obtain a geometrical model of the branching structure with depth, as represented in Figure 10c. The actual vertical scaling requires independent geological constraints.

[38] The first constraint corresponds to the maximum depth of the hydrothermal reaction zone, and therefore the base of the hydrothermal upflow system. The Lucky Strike site is located above an AMC (Figure 1), and its seismically imaged roof, located ∼3 km below the seafloor [*Singh et al.*, 2006] is likely the deeper limit of the system.

[39] The main split of the hydrothermal discharge (E versus W sites), visible in the distance maps (Figures 10a and 10b) and in the clustering, is clearly associated with the faults (Figure 8a) [*Ondréas et al.*, 2009; *Tolstoy et al.*, 2008] that bound the central graben. Upwelling hydrothermal fluids thus likely exploit high-permeability zones associated with the fault networks at both flanks of the graben, efficiently steering the fluids away from its axis (Figure 11a). An estimate of this E-W branching depth (Figure 10c) may be obtained from intersection of faults at depth. Assuming that the 1 km-wide graben is symmetrical, and that faults dip between 45° to 60° [e.g., *Thatcher and Hill*, 1995], the depth of fault intersection (and therefore fluid divergence) may vary between ∼500 m and 900 m (Figure 10c and 11a).
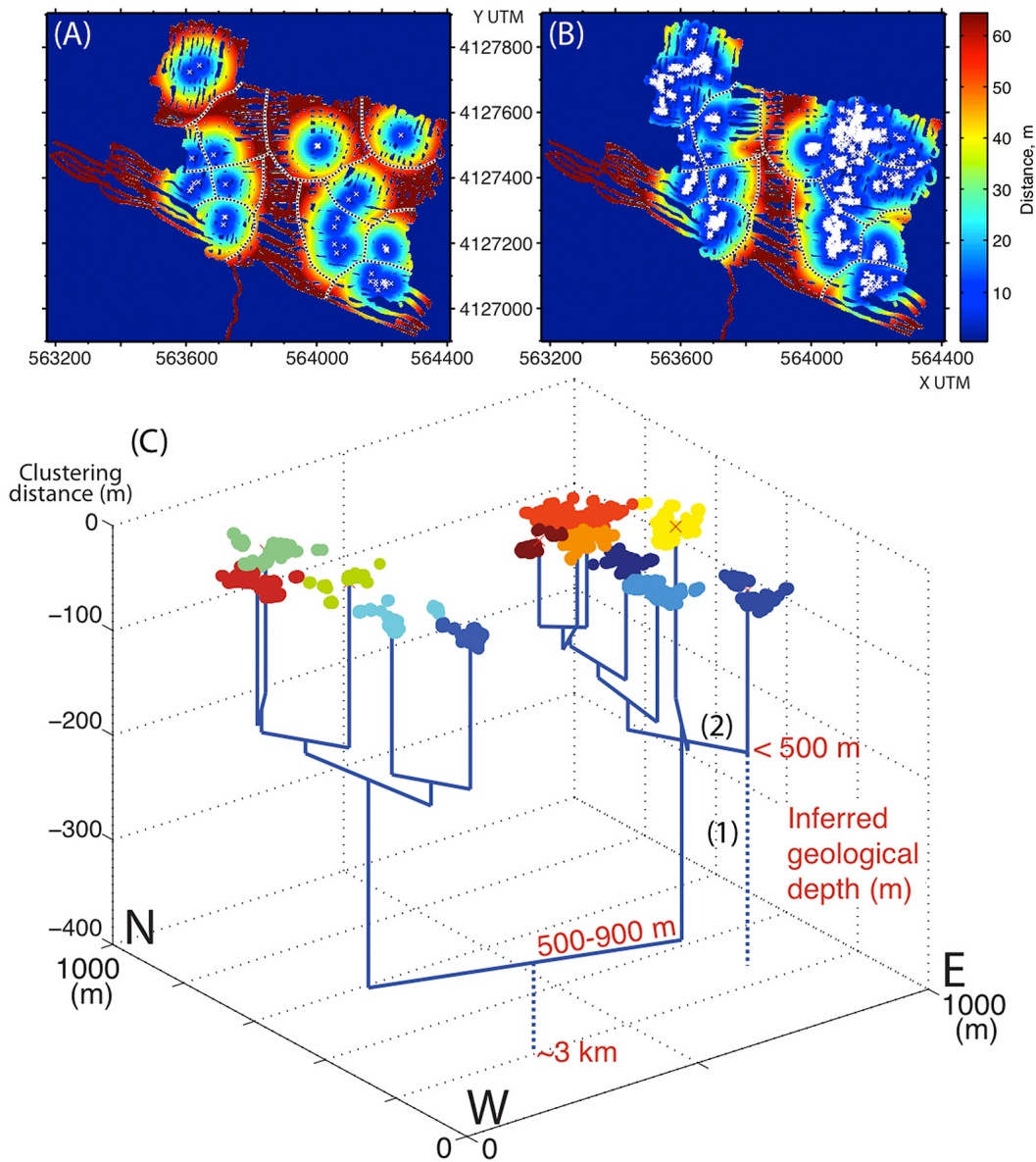
Figure 10. (top) Maps of distance to (a) the nearest focused vent or (b) diffuse outflow feature, with interpreted primary outflow zones (dashed lines). (c) Plumbing structure interpreted from a clustering analysis of diffuse hydrothermal outflow features (see text for details). The distance between the centers of the different clusters is assumed to be a proxy for the vertical dimension (clustering distance, black in Figure 10c) of the underlying plumbing system. Actual depths inferred from geological constraints, given in red, correspond to a) the base of the hydrothermal system (top of the AMC, ~3000 m); b) the main split of the outflow (E and W) at the intersection of rift bounding faults at depth (500–900 m); and c) shallow-level branching along faults at inferred depths of <500 m. (1) and (2) numbers correspond to two different hypothesis for clustering: chemical differences in hydrothermal fluids are (1) due to two different fluid sources in depth or (2) associated with nature of the different substrates.

[40] The apparent clustering of hydrothermal activity (Figure 10c) suggests a further organization of the outflow along smaller channels at levels shallower than the 500 m–900 m inferred for the main E-W fault split. These outflows are directly linked to the shallow fault network within each of the fault branches of the graben. Lacking direct depth constraints, we estimate that characteristic depths may correspond to half of the branching depth (500–200 m) or less (Figures 10c and 11b).

[41] The inferred plumbing system is based on the spatial structure of outflow zones, and does not take
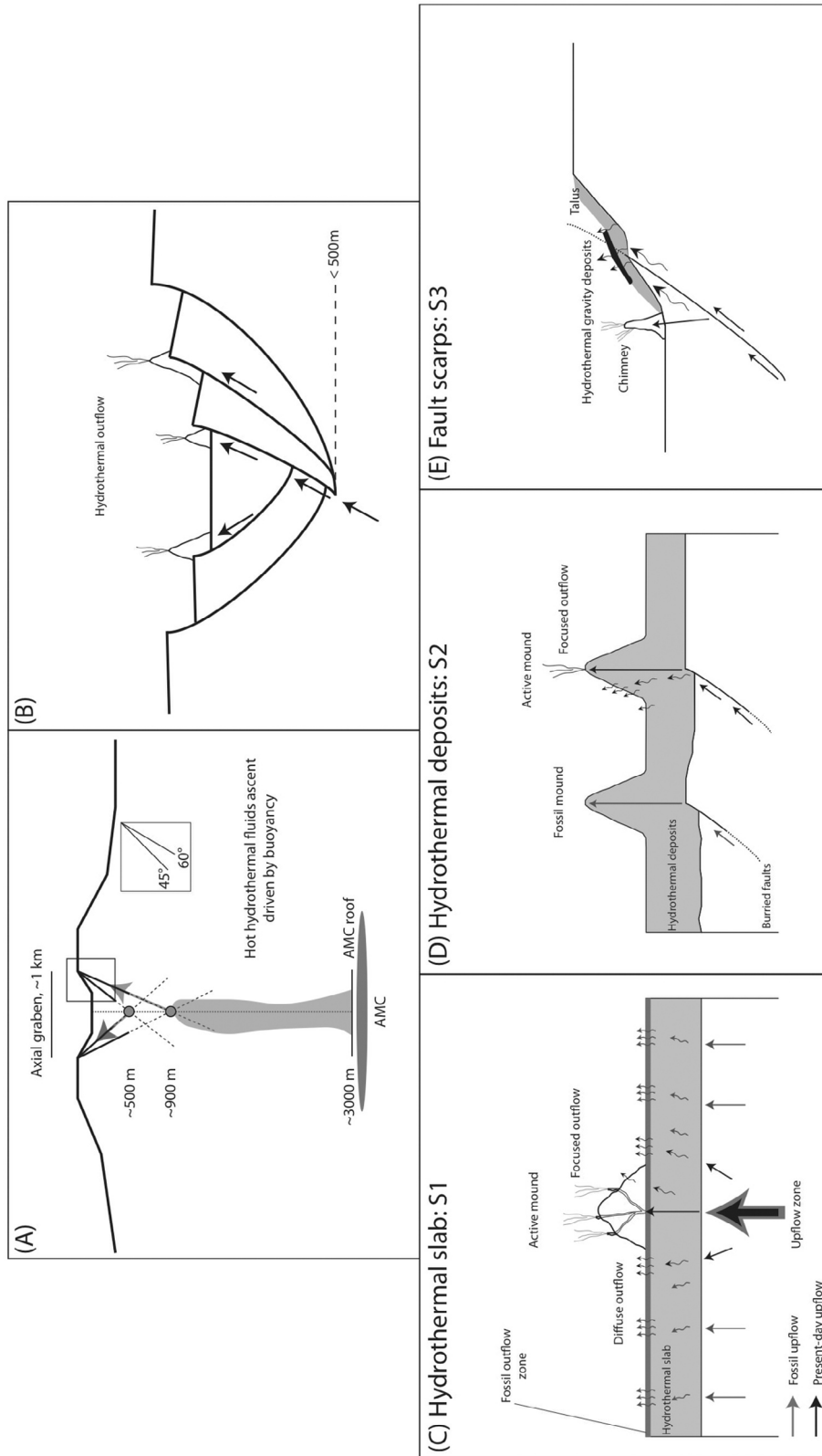
Figure 11. (a) Conceptual model of the Lucky Strike hydrothermal plumbing system structure at depth, with the upwelling of a single plume above the AMC that is focused along high-porosity areas associated with the main faults bounding the axial graben. The maximum depth of this branching may be constrained by the intersection of the bounding faults, here assumed to dip between 45° and 60°. (b) At shallower levels, hydrothermal outflow in the E and W exploits existing smaller-scale faults, as suggested by the association of hydrothermal features and fault scarps. The nature of the discharge at the scale of individual sites is likely controlled by the permeability structure of the crust immediately below the seafloor (<100 m²). In the presence of (c) the hydrothermal "slab" substrate sites tend to display a high-temperature discharge zone (vents in mounds or chimneys), with diffuse outflow in surrounding areas. In the presence of (d) hydrothermal deposits, faults acting as fluid conduits may be buried. Discharge thus occurs through hydrothermal rubble. (e) Fault scarps show evidence of mass wasting, and are likely associated with a layer of unconsolidated and heterogeneous material, in which hydrothermal discharge takes place.

into account other information such as the geo-chemistry of fluids. The SE hydrothermal sites (e.g., Tour Eiffel and Montsegur) display a fluid geochemistry that indicates a different fluid source from the rest of the Lucky Strike sites [*Langmuir et al.*, 1997; *Von Damm et al.*, 1998; *Charlou et al.*, 2000]. If these geochemical differences are associ-ated with reaction zones that are distinct at depth, the plumbing system would require that these sites root independently (dashed line, Figure 10c). Alternatively, these chemical differences may be caused instead by the nature of the substrate and chemical reactions within the upwelling zone, and thus may be consistent with the plumbing system proposed here.

[42] Variations in the style of venting associated with the various substrates throughout the Lucky Strike field (Figure 7) suggest that the permeable structure of the crust immediately below the sea-floor may control hydrothermal outflow throughout (Figure 11c–11e). Most of the discharge from the slab substrate is organized around a chimney or mound hosting high temperature vents, and sur-rounded by diffuse outflow (Figure 11c). The rela-tive size of the area with diffuse outflow is highly variable, and we find no correlation with the nature and number of high-temperature vents associated with it.

[43] The nature of the present-day hydrothermal outflow and its relation to structure is more clearly defined in the south of the hydrothermal field, hos-ted by the slab substrate. Mixing and dispersion of high-temperature fluids may occur at the base of the slab, and move away from the focused venting areas through percolation along cracks [e.g., *Cooper et al.*, 2000]. In contrast, along the slopes of both fault scarps and inactive hydrothermal mounds, focused venting is currently scarce and diffuse out-flow results in ill-defined clusters of actively vent-ing areas. In these zones the subsurface is composed of rubble and unconsolidated materials (talus), possibly promoting the dispersion of hydrothermal fluids (Figure 11d–11e). The lack of a systematic association between the type of diffuse discharge and substrate indicates that other parameters may play a role, such as the size of individual discharge zones at depth and their flux.

5.2. Heat Flux Estimates Using Seafloor Imagery

[44] Heat flux, and its partition between focused and diffuse outflow, may be estimated from the area of venting, constrained by the mosaics presented here,

in addition to the temperature of the fluids, and their average outflow speed, based on prior studies [*Cooper et al.*, 2000; *Sarrazin et al.*, 2009; *Mittelstaedt et al.*, 2012]. Available heat flux esti-mates based upon water column studies of the hydrothermal plume for the Lucky Strike hydro-thermal field vary by an order of magnitude. *Wilson et al.* [1996] estimated it at 118–399 MW based on plume height modeling and buoyancy arguments. *Jean Baptiste et al.* [1998] propose a much higher value of 3800 ± 1200 MW, based on ^{3}He analyses of the plume and its relationship to heat flux.

[45] Focused hydrothermal outflow through vents can be evaluated for the whole field using heat flux calculated for individual vents. Tour Eiffel is the only location where detailed heat flux measure-ments have been performed, based on temperature measurements and video estimates of fluid veloci-ties [e.g., *Mittelstaedt et al.*, 2012], yielding an average heat flux of ~0.12 MW per focused vent. This estimate is significantly lower than the inferred ~0.8 MW of focused vents at the EPR, measured with flowmeters [*Ramondenc et al.*, 2006]. As no systematic study has been perform throughout the entire hydrothermal field, using these two heat flux estimates as minimum and maximum values, and based on the number of identified sites (67), we estimate that the focused flow observable at the present time may be between ~8 and 50 MW.

[46] The heat flux associated with diffuse flow and cracks is poorly constrained, owing to the variability and heterogeneity in the temperatures and velocities of fluids, even at small spatial scales. Heat flux may be calculated from

$$Q = \Delta T \times \phi \times v \times C_p \times S \qquad (1)$$

where ϕ is density of seawater (1025 kg.m^{-3}), C_p is the specific heat of the diffuse fluid (4.2 10^3 J. kg^{-1}.$°$C^{-1}), ΔT is temperature difference $T–T_0$ between outflow temperature T and ambient sea-water T_0 (4.4°C), v is the diffuse effluent velocity, and S the area of considered diffuse outflow (m^2) which is constrained from the image mosaic (see Table 4).

[47] Data on velocity and temperature of diffuse fluids is limited, and thus we use a broad range of plausible values to obtain a range of field-based heat-flux estimates for each of type of dif-fuse outflow. *Sarrazin et al.* [2009] deployed a flowmeter over patches of bacterial mats at Lucky Strike, yielding minimum and maximum tempera-tures of 8° and 20°C, and minimum and maximum

Table 4. Heat Flux Estimates (Q) Associated With Diffuse Outflow at the Lucky Strike Hydrothermal Field, Based on Measured Surface Area (S), Temperature (T) and Velocity (V) for Each Type of Diffuse Outflow[a]

	S^b (m^2)	T_{min}/T_{max} (°C)	V_{min}/V_{max} (mm/s)	Q_{min}/Q_{max} (MW)
Patch	975	8[c]/20[c]	1[c]/5[c]	15/327
Mound	630	8[c]/20[c]	1[c]/5[c]	10/212
Cracks	144	17.5[d]/33[e]	19[e]/21[d]	154/372
Streaks	20	100[f]/150[f]	1[c]/10[f]	8/125
Total				187/1036

[a]Minimum and maximum (min and max respectively) values of T, V and Q are given.
[b]From this study.
[c]From *Sarrazin et al.* [2009].
[d]From *Mittelstaedt et al.* [2012].
[e]From *Cooper et al.* [2000].
[f]Temperatures inferred from *Møller* [1988] and *Bischoff and Seyfried* [1978]. The maximum velocity is arbitrarily set to double of the maximum velocity reported by *Sarrazin et al.* [2009] (see text for discussion).

velocities of 1 to 5 mm/s, which we apply to both patches and mounds owing to the similarity in type of outflow. We obtain a range of heat fluxes of 15 to 327 MW for the patches, and of 10 to 212 MW for the mounds (Table 4). Flowmeter measurements along cracks have been performed at Lucky Strike by *Cooper et al.* [2000]. A total of 10 measurements throughout the field yield an average temperature and fluid flow velocity of 33°C and 19 mm/s respectively. More recent experiments were carried out at the Tour Eiffel site (MOMAR'08 and Bathyluck'09 cruises [*Mittelstaedt et al.*, 2012]) yielded average temperatures of 17.5°C and similar outflow velocities of 21 mm/s (Table 4). We thus estimate that heat fluxes associated with cracks range from 154 to 372 MW. Our heat flux estimate for streaks is the least constrained, lacking any direct measurements. The outflow fluid temperatures associated with these structures may range from 100°C to 150°C, which are used as the minimum and maximum for the heat flux estimate in Table 4, so as to allow the formation of anhydrate [*Møller*, 1988; *Bischoff and Seyfried*, 1978]. These elevated temperatures, in the absence of significant mixing at the source, may also preclude the development of bacterial mats. Examination of video imagery from transits over these areas shows no significant or pervasive simmering, nor the presence of plumes indicating elevated flow rates. To fully cover the range of likely values in the field, and lacking direct measurements, we arbitrarily adopt as a minimum that of *Sarrazin et al.* [2009] of 1 mm/s, and a maximum speed equal to twice that reported by these authors, 10 mm/s. Based on these assumptions, we obtain a broad range of heat fluxes, from 8 to 125 MW.

[48] Combining all these results, our best estimates of the heat flux for the entire Lucky Strike field range from 187 to 1036 MW for diffuse areas, and from 8 to 50 MW for focused vents, yielding a total heat flux of 195–1086 MW. Based on the distribution of active venting areas, we also predict a strong asymmetry in heat flux across axis, with ~70% of it being delivered on the East flank. These mosaic-based heat flux estimates are closer to those of *Wilson et al.* [1996] (118–399 MW), and suggest that He-based estimates [*Jean-Baptiste et al.*, 1998] (3800 ± 1200 MW) are an overestimate, probably due to the limitations and assumptions involved.

5.3. Decline of Lucky Strike Hydrothermal Activity

[49] Image mosaics document a systematic and widespread decline of diffuse hydrothermal outflow at Lucky Strike over the last 13 years, which we attribute to an overall reduction in the mass flux of hydrothermal discharge across field. Diffuse outflows result from mixing of ascending, high-temperature hydrothermal fluids with seawater within the shallow, permeable crust. Based solely on outflow temperature, the diffuse venting contains a small fraction of hydrothermal fluids (e.g., <10% for a 10°C outflow resulting from mixing of cold seawater and 300°C fluids). Diffuse venting is thus sensitive to small variations in the overall hydrothermal flux at depth, which may be due to either a reduction of the upflow speed, a decrease in the size (diameter) of discharge zones and hence of the associated mixing zone surrounding them, or both. The temporal variability that we report here is qualitative, and lacking other independent measurements (e.g., systematic estimates based on plume studies at the scale of the site) we cannot quantify the heat flux reduction over this time span. However, based on the stability of the location of the outflow zones and of their geometry, as well as on the local nature of these changes, we propose that the observed decadal-scale decline is small relative to the overall heat flux of the site.

[50] Temperature measurements over the last 20 years (Table 5) at the Tour Eiffel, Sintra, and Y3 sites, in addition to the now extinct Statue of Liberty (measurements available in 1993 and 1994, and extinct by 2009) support this interpretation. Each of the now active sites is located on a different substrate type (S1, S2 and S3, respectively, Figure 7). Table 5 reports the highest temperatures measured at any given year for each of the sites

Table 5. In Situ Measurements of High-Temperature Outflow at Selected Hydrothermal Vents From the Lucky Strike Field (Temperatures in °C)[a]

	1993[b]	1994[c]	1996[d]	1997[e]	2008[f,g]	2009[g]	2010[g]	2011[g]	Average ± STD[h]
Tour Eiffel	325	324	323	324	*184*[g]	317	*296*	325	323.0 ± 3.0
Sintra	212	215	222	*176*	200[f]	217		207	302.3 ± 7.8
Y3	333	324	328		319[f]	321			325.0 ± 5.6
Statue of Liberty	202	185				Extinct			

[a]Numbers in italics correspond to values significantly lower than the average, and that we attribute to measurements within the mixing zone of seawater and hydrothermal fluids.
[b]FAZAR cruise [*Langmuir et al.*, 1997].
[c]DIVA 1 cruise [*Charlou et al.*, 2000].
[d]LUSTRE cruise [*Von Damm et al.*, 1998; *Charlou et al.*, 2000].
[e]Flores cruise [*Charlou et al.*, 2000].
[f]KNOX18RR cruise (data from WHOI Deep Submergence database, JASON VirtualVan available at http://4dgeo.whoi.edu/jason/).
[g]This study, from cruises MoMAR (2008), Bathyluck (2009), MoMARSAT (2010 and 2011).
[h]Average and standard deviation do not include the temperatures in italics, that are considered anomalously low.

available in the literature. We have excluded some anomalously low values, that show departures of 30°C and up to >100°C, which we attribute to measurements performed within the mixing zone and thus not corresponding to the high-temperature fluids. The remaining outflow temperatures have been very stable, and show variations of <15°C (e.g., 325°C in 1993 and 2009 for Tour Eiffel), although we cannot determine if there have been volume flux variations over this same period of time.

[51] The short-term decline in diffuse outflow is consistent with an apparent decrease in the extent and intensity of hydrothermal activity at longer periods of time, as interpreted from observations in S and E of the Lucky Strike site, over the S1 and S2 substrates. Inferences of temporal evolution on fault scarps (S3) are hindered by the inherently unstable nature of these areas, characterized by mass wasting on talus. Identified fossil hydrothermal outflow (dark areas of the seafloor in S1, and extinct hydrothermal constructions in S2) occurred over a larger area than that of the present-day activity. For example, in the 'slab' substrate (S1) the fossil outflow zones cover an area an order of magnitude larger than the present-day diffuse outflow area (Figure 6). While we lack dating to constrain the age of fossil hydrothermal structures here (chimneys, bulbous features), we estimate a maximum age, based upon spreading (~10 km/Ma) and distance from the graben axis (~300 m for the furthest sites), at ~30,000 years. This area has been resurfaced by recent volcanic eruptions, as demonstrated by the volcanic history at the lava lake [*Ondréas et al.*, 2009], and thus the actual age may be considerably younger. We propose that the age of these fossil outflow zones likely spans between a few thousands of years to a

few tens of thousands of years [e.g., *Humphris et al.*, 2002], sufficient to allow the formation and death of the largest hydrothermal chimneys and mounds that are now extinct in the area. The systematic occurrence of present-day activity within the fossil outflow zones suggests a significant reduction of the surface area of both focused and diffuse hydrothermal outflow that may be linked to an overall mass and heat flux reduction throughout the field. This interpretation is consistent with the shorter-term decline documented from imagery.

[52] Alternatively, a translation with time of the hydrothermal activity would also yield large areas of fossil outflow. However, based on a) the geometrical association of inactive and active flow within former outflow areas over substrate S1, b) the well-defined limits of these fossil outflow zones, and c) the consistent decline in activity over the last ~20 years, our preferred interpretation is an overall and continuous decline of the site. Furthermore, we observe no reactivation or appearance of new sites, nor active sites outside the dark areas in S1, which would be expected with spatial shifting of the outflow at the seafloor.

[53] While the underlying causes of the decline in hydrothermal activity are not well known, the heat extracted by the hydrothermal discharge at the Lucky Strike field is likely associated with the cooling and crystallization of melt in the underlying magma chamber. We consider now two values of heat flux, a lower bound of ~100 MW based upon the minimum estimate of *Wilson et al.* [1996], and upper bound using our maximum estimate of ~1000 MW. Assuming a latent heat of crystallization for basalt of 0.5 MJ/kg [*Kojitani and Akaogi*, 1997] and a melt density of 2800 kg/m³, these heat flux estimates would thus represent the crystallization of 2.3–22.5 × 10⁶ m³/yr of melt. Seismic

observations suggest that the AMC extends ~6 km along-axis and ~2 km across-axis [*Singh et al.*, 2006; *Combier*, 2007]. If crystallization were distributed throughout the melt lens, the heat flux can potentially represent the freezing of a melt thickness of 0.2–1.9 m/year. Neither the thickness nor the volume of melt of the Lucky Strike AMC are well constrained, but assuming an AMC thickness of 200 m, similar to that inferred at the EPR [e.g., *Collier and Singh*, 1998], with 100% melt (i.e., no previous crystallization), and no magma recharge events, the melt lens would freeze in 100–1000 years. A slower rate of melt freezing time may be achieved if the heat were mined from other areas along the axis and not solely from the AMC [e.g., *Fontaine et al.*, 2008], and/or by replenishment of the magma chamber. We expect that, at longer time scales, this AMC replenishment will result in volcanic eruptions and resurfacing of the seafloor, in addition to a resetting of the hydrothermal system at the segment center. The recurrence time of such magmatic events is unknown, but we speculate that it would be up to several orders of magnitude longer than the observed decline of hydrothermal activity reported here (1000 to 10s of thousands of years).

6. Conclusions

[54] We have demonstrated that repeated photographic surveys of the seafloor using video and electronic still cameras can be used to construct image mosaics over large areas of the seafloor. New image processing techniques also allow us to geographically register repeated surveys that can then be used for temporal studies. We applied these techniques at the Lucky Strike hydrothermal field to construct mosaics with a resolution of <10 mm and covering an area of ~1 km^2.

[55] We have identified four types of diffuse outflow (hydrothermal mounds, diffuse patches, cracks, and streaks of hydrothermal deposits on slopes) from image mosaics. Outflow type and venting area seem to be correlated with the nature of the substrate. We find more focused and organized outflow in areas where the hydrothermal 'slab' is present, whereas outflow through older hydrothermal deposits and fault scarps is characterized by a relatively low number of high-temperature vents, and more pervasive diffuse outflow. We interpret dark seafloor patches containing dead hydrothermal structures as areas of fossil hydrothermal outflow, within which the present-day hydrothermal activity concentrates.

[56] The geometry of hydrothermal discharge at the seafloor reveals a pattern of clustering that we suggest reflects the underlying plumbing system at depth. Two main venting areas are observed, E and W, probably controlled by the set of faults bounding the axial graben, and redistribution of outflow at shallow levels exploits existing faults (90% of outflow structures are within 20 m of a fault scarp).

[57] Quantification of both the number of vents and the surface area with diffuse venting, in combination with field measurements, allow us to provide independent constraints on the total heat flux at Lucky Strike. We estimate that the total heat flux is between ~200 MW and 1000 MW, with 75% to 90% of it taken up by diffuse outflow. We also estimate that the activity is concentrated in the E where ~70% of the hydrothermal discharge appears to take place.

[58] Repeated image surveys reveal a decline in the intensity of diffuse hydrothermal outflow at the Lucky Strike field over the last 10–20 years, consistent with an apparent longer-term decrease. We speculate that this decline may be explained by the cooling of the AMC, as our heat flux estimates suggest that the AMC will freeze within ~100–1000 years if there is no magmatic replenishment.

Acknowledgments

References

Alt, J. C. (1995), Subseafloor processes in mid-ocean ridge hydrothennal systems, in *Seafloor Hydrothermal Systems: Physical, Chemical, Biological, and Geological Interactions*, *Geophys. Monogr. Ser.*, vol. 91, edited by S. E. Humphris et al., pp. 85–114, AGU, Washington, D. C., doi:10.1029/GM091p0085.

Baker, E. T. (2007), Hydrothermal cooling of mid ocean ridge axes: Do measured and modeled heat fluxes agree?, *Earth Planet. Sci. Lett.*, *263*, 140–150, doi:10.1016/j.epsl.2007.09.010.

Baker, E. T., G. Massoth, S. Walker, and R. W. Embley (1993), A method for quantitatively estimating diffuse and discrete hydrothermal discharge, *Earth Planet. Sci. Lett.*, *118*, 235–249, doi:10.1016/0012-821X(93)90170-E.

Ballu, V., et al. (2009), A seafloor experiment to monitor vertical deformation at the Lucky Strike volcano, Mid-Altantic Ridge, *J. Geod.*, *83*, 147–159, doi:10.1007/s00190-008-0248-3.

Bischoff, J. L., and W. E. Seyfried (1978), Hydrothermal chemistry of seawater from 25° to 350°C, *Am. J. Sci.*, *278*, 838–860, doi:10.2475/ajs.278.6.838.

Bohnenstiehl, D., and M. C. Kleinrock (2000a), Evidence of spreading-rate dependence in the displacement-length ratios of abyssal hill faults at mid-ocean ridges, *Geology*, *28*, 395–398, doi:10.1130/0091-7613(2000)28<395:EFSDIT>2.0.CO;2.

Bohnenstiehl, D. R., and M. C. Kleinrock (2000b), Fissuring near the TAG active hydrothermal mound 26°N on the Mid-Atlantic Ridge, *J. Volcanol. Geotherm. Res.*, *98*, 33–48, doi:10.1016/S0377-0273(99)00192-4.

Brundage, W. L., and R. B. Patterson (1976), LIBEC photography as a sea floor mapping tool, in *Oceans'76*, pp. 156–166, Mar. Technol. Soc., Washington, D. C.

Brüning, M., H. Sahling, I. R. MacDonald, F. Ding, and G. Bohrmann (2010), Origin, distribution, and alteration of asphalts at Chapopote Knoll, Southern Gulf of Mexico, *Mar. Pet. Geol.*, *27*, 1093–1106, doi:10.1016/j.marpetgeo.2009.09.005.

Cannat, M., et al. (1999), Mid-Atlantic ridge–Azores hotspot interactions: Along-axis migration of a hotspot-derived magmatic pulse 14 to 4 myrs ago, *Earth Planet. Sci. Lett.*, *173*, 257–269, doi:10.1016/S0012-821X(99)00234-4.

Charlou, J. J., J. P. Donval, E. Douville, P. Jean Baptiste, J. Radford-Knoery, Y. Fouquet, A. Dapoigny, and M. Stievenard (2000), Compared geochemical signatures and the evolution of Menez Gwen (37°50′N) and Lucky Strike (37°17′N) hydrothermal fluids, south of the Azores Triple Junction on the Mid-Atlantic Ridge, *Chem. Geol.*, *171*, 49–75, doi:10.1016/S0009-2541(00)00244-8.

Colaço, A., et al. (2011), MoMAR-D: A technological challenge to monitor the dynamics of the Lucky Strike vent ecosystem, *ICES J. Mar. Sci.*, *68*, 416–424, doi:10.1093/icesjms/fsq075.

Collier, J. S., and S. C. Singh (1998), A seismic inversion study of the axial magma chamber reflector beneath the East Pacific Rise near 10°N, in *Modern Ocean Floor Processes and the Geological Record*, edited by R. A. Mills and K. Harrison, *Geol. Soc. Spec. Publ.*, *148*, 17–28.

Combier, V. (2007), *Mid-ocean Ridge Processes: Insights From 3D Reflection Seismics at the 9°N OSC on the East Pacific Rise, and the Lucky Strike Volcano on the Mid-Atlantic Ridge*, 261 pp., Inst. de Phys. du Globe, Paris.

Cooper, M. J., H. Elderfield, and A. Schultz (2000), Diffuse hydrothermal fluids from Lucky Strike hydrothermal vent field: Evidence for a shallow conductively heated system, *J. Geophys. Res.*, *105*(B8), 19,369–19,375, doi:10.1029/2000JB900138.

Cuvelier, D., J. Sarrazin, A. Colaço, J. Copley, D. Desbruyères, A. G. Glover, P. Tyler, and R. S. Santos (2009), Distribution and spatial variation of hydrothermal faunal assemblages at Lucky Strike (Mid-Atlantic Ridge) revealed by high-resolution video image analysis, *Deep Sea Res., Part I*, *56*, 2026–2040, doi:10.1016/j.dsr.2009.06.006.

DeMets, C., R. G. Gordon, D. F. Argus, and S. Stein (1990), Current plate motions, *Geophys. J. Int.*, *101*, 425–478, doi:10.1111/j.1365-246X.1990.tb06579.x.

Desbruyères, D., et al. (2001), Variations in deep-sea hydrothermal vent communities on the Mid-Atlantic ridge near the Azores plateau, *Deep Sea Res., Part I*, *48*, 1325–1346, doi:10.1016/S0967-0637(00)00083-2.

Dziak, R. P., D. K. Smith, D. R. Bohnenstiehl, C. G. Fox, D. Desbruyères, H. Matsumoto, M. Tolstoy, and D. J. Fornari (2004), Evidence of a recent magma dike intrusion at the slow spreading Lucky Strike segment, Mid-Atlantic Ridge, *J. Geophys. Res.*, *109*, B12102, doi:10.1029/2004JB003141.

Elderfield, H., and A. Schultz (1996), Mid-ocean ridge hydrothermal fluxes and the chemical composition of the ocean, *Annu. Rev. Earth Planet. Sci.*, *24*, 191–224, doi:10.1146/annurev.earth.24.1.191.

Emmanuel, S., and B. Berkowitz (2006), Suppression and stimulation of seafloor hydrothermal convection by exothermic mineral hydration, *Earth Planet. Sci. Lett.*, *243*, 657–668, doi:10.1016/j.epsl.2006.01.028.

Escartín, J., M. Cannat, G. Pouliquen, A. Rabain, and J. Lin (2001), Crustal thickness of V-shaped ridges south of the Azores: Interaction of the Mid-Atlantic Ridge (36°–39°N) and the Azores hot spot, *J. Geophys. Res.*, *106*, 21,719–21,735, doi:10.1029/2001JB000224.

Escartín, J., et al. (2008a), Globally aligned photo mosaic of the Lucky Strike hydrothermal Vent Field (Mid-Atlantic Ridge, 37°18.5′N): Release of geo-referenced data, mosaic construction and viewing software, *Geochem. Geophys. Geosyst.*, *9*, Q12009, doi:10.1029/2008GC002204.

Escartín, J., D. K. Smith, J. Cann, H. Schouten, C. H. Langmuir, and S. Escrig (2008b), Central role of detachment faults in accretion of slow-spreading oceanic lithosphere, *Nature*, *455*, 790–794, doi:10.1038/nature07333.

Fisher, A. T., and K. Becker (1991), Heat flow, hydrothermal circulation and basalt intrusions in the Guaymas Basin, Gulf of California, *Earth Planet. Sci. Lett.*, *103*, 84–99, doi:10.1016/0012-821X(91)90152-8.

Foley, B. P., et al. (2009), The 2005 Chios ancient shipwreck survey. New methods for underwater archaeology, *Hesperia*, *78*, 269–305, doi:10.2972/hesp.78.2.269.

Fontaine, F. J., and W. S. D. Wilcock (2007), Two-dimensional numerical models on open-top hydrothermal convection on high Rayleigh and Nusselt numbers: Implications for mid-ocean ridge hydrothermal circulation, *Geochem. Geophys. Geosyst.*, *8*, Q07010, doi:10.1029/2007GC001601.

Fontaine, F. J., M. Cannat, and J. Escartín (2008), Hydrothermal circulation at slow-spreading mid-ocean ridges: The role of along-axis variations in axial lithospheric thickness, *Geology*, *36*, 759–762, doi:10.1130/G24885A.1.

Fontaine, F. J., S. D. Wilcock, D. I. Foustoukos, and D. A. Butterfield (2009), A Si-Cl geothermobarometer for the reaction zone of high-temperature, basaltic-hosted mid-ocean ridge hydrothermal systems, *Geochem. Geophys. Geosyst.*, *10*, Q05009, doi:10.1029/2009GC002407.

Fornari, D. J. (2003), A new deep-sea towed digital camera and multi-rock coring system, *Eos Trans. AGU*, *84*, 69–76, doi:10.1029/2003EO080001.

Fouquet, Y., H. Ondréas, J.-L. Charlou, J.-P. Donval, J. Radford-Knoery, I. Costa, N. Lourenco, and M. K. Tivey (1995), Atlantic lava lakes and hot vents, *Nature*, *377*, 201, doi:10.1038/377201a0.

Garcia, R., R. Campos, and J. Escartín (2011), High-resolution 3D reconstruction of the seafloor for environmental monitoring and modelling, paper presented at IEEE/RSJ International Conference on Intelligent Robots and Systems, Workshop on Robotics for Environmental Monitoring, Inst. of Electr. and Electron. Eng., San Francisco, Calif.

German, C. R., et al. (2010a), Diverse styles of submarine venting on the ultraslow spreading Mid-Cayman Rise, *Proc. Natl. Acad. Sci. U. S. A.*, *107*, 14,020–14,025, doi:10.1073/pnas.1009205107.

German, C., A. M. Thurnherr, J. Knoery, J.-L. Charlou, P. Jean-Baptiste, and H. N. Edmonds (2010b), Heat, volume and chemical fluxes from submarine venting: A synthesis of results from the Rainbow hydrothermal field 36°N MAR, *Deep Sea Res., Part I*, *57*(4), 518–527, doi:10.1016/j.dsr.2009.12.011.

Haymon, R. M., K. C. Macdonald, S. B. Benjamin, and C. J. Ehrhardt (2005), Manifestations of hydrothermal discharge from young abyssal hills on the fast-spreading East Pacific Rise flank, *Geology*, *33*, 153–156, doi:10.1130/G21058.1.

Humphris, S. E., Fornari, D. J., Scheirer, D. S., German, C. R., and Parson, L. M. (2002), Geotectonic setting of hydrothermal activity on the summit of Lucky Strike seamount (37°17′N, Mid-Atlantic Ridge), *Geochem. Geophys. Geosyst.*, *3*(8), 1049, doi:10.1029/2001GC000284.

Jean-Baptiste, P., H. Bougault, A. Vangriesheim, J.-L. Charlou, J. Radford-Knoery, Y. Fouquet, H. D. Needham, and C. German (1998), Mantle ^{3}He in hydrothermal vents and plume of the Lucky Strike site (MAR 37°17′N) and associated geothermal heat flux, *Earth Planet. Sci. Lett.*, *157*, 69–77, doi:10.1016/S0012-821X(98)00022-3.

Kleinrock, M. C., and S. E. Humphris (1996), Structural asymmetry of the TAG rift valley: Evidence from a near-bottom survey for episodic spreading, *Geophys. Res. Lett.*, *23*, 3439–3442, doi:10.1029/96GL03073.

Kojitani, H., and M. Akaogi (1997), Melting enthalpies of mantle peridotite: Calorimetric determinations in the system CaO-MgO-Al$_2$O$_3$-SiO$_2$ and application to magma generation, *Earth Planet. Sci. Lett.*, *153*, 209–222, doi:10.1016/S0012-821X(97)00186-6.

Langmuir, C. H., et al. (1993), Geological setting and characteristics of the Lucky Strike vent field at 37°17′N on the Mid-Atlantic Ridge, *Eos Trans. AGU*, *74*, 99.

Langmuir, C., et al. (1997), Hydrothermal vents near a mantle hot spot: The Lucky Strike vent field at 37°N on the Mid-Atlantic Ridge, *Earth Planet. Sci. Lett.*, *148*, 69–91, doi:10.1016/S0012-821X(97)00027-7.

Lessard-Pilon, S., M. D. Porter, E. E. Cordes, I. MacDonald, and C. R. Fisher (2010), Community composition and temporal change at deep Gulf of Mexico cold seeps, *Deep Sea Res., Part II*, *57*, 1891–1903, doi:10.1016/j.dsr2.2010.05.012.

Lister, C. R. B. (1982), "Active" and "passive" hydrothermal systems in the ocean crust. Predicted physical conditions, in *The Dynamic Seafloor*, edited by K. A. Fanning and F. T. Manheim, pp. 441–470, Heath, Lexington, Mass.

Lundsten, L., K. L. Schlining, K. Frasier, S. B. Johnson, L. A. Kuhnz, J. B. J. Harvey, G. Clague, and R. C. Vrijenhoek (2010), Time-series analysis of six wale-fall communities in Monterey Canyon, California, USA, *Deep Sea Res., Part I*, *57*, 1573–1584, doi:10.1016/j.dsr.2010.09.003.

Maki, T., H. Kondo, T. Ura, and T. Sakamaki (2008), Large-area visual mapping of an underwater vent field using the AUV "Tri-Dog 1", in *Oceans 2008*, pp. 1135–1702, IEEE Press, Piscataway, N. J.

Martins, I., A. Colaço, R. S. Santos, F. Lesongeur, A. Godfroy, P.-M. Sarradin, and R. P. Cosson (2009), Relationship between the occurrence of filamentous bacteria on *Bathymodiolus azoricus* shell and the physiological and toxicological status of vent mussel, *J. Exp. Mar. Biol. Ecol.*, *376*, 1–6, doi:10.1016/j.jembe.2009.05.001.

McCaig, A., R. A. Cliff, J. Escartín, A. E. Fallick, and C. J. MacLeod (2007), Oceanic detachment faults focus very large volumes of black smoker fluids, *Geology*, *35*, 935–938, doi:10.1130/G23657A.1.

Mittelstaedt, E., J. Escartín, N. Gracias, J.-A. L. Olive, T. Barreyre, A. Davaille, M. Cannat, and R. Garcia (2012), Quantifying diffuse and discrete venting at the Tour Eiffel vent site, Lucky Strike hydrothermal field, *Geochem. Geophys. Geosyst.*, *13*, Q04008, doi:10.1029/2011GC003991.

Miranda, J. M., J. F. Luis, N. Lourenço, and F. M. Santos (2005), Identification of the magnetization low of the Lucky Strike hydrothermal vent using magnetic data, *J. Geophys. Res.*, *110*, B04103, doi:10.1029/2004JB003085.

Møller, N. (1988), The prediction of mineral solubilities in natural waters: A chemical equilibrium model for the Na-Ca-Cl-SO$_4$–H$_2$O system, to high-temperature and concentration, *Geochim. Cosmochim. Acta*, *52*, 821–837, doi:10.1016/0016-7037(88)90354-7.

Ondréas, H., Y. Fouquet, M. Voisset, and J. Radford-Knoery (1997), Detailed study of three contiguous segments of the Mid-Atlantic Ridge, South of the Azores (37°N to 38°30′N), using acoustic imaging coupled with submersible observations, *Mar. Geophys. Res.*, *19*, 231–255, doi:10.1023/A:1004230708943.

Ondréas, H., M. Cannat, Y. Fouquet, A. Normand, P.-M. Sarradin, and J. Sarrazin (2009), Recent volcanic events and the distribution of hydrothermal venting at the Lucky Strike hydrothermal field, Mid-Atlantic Ridge, *Geochem. Geophys. Geosyst.*, *10*, Q02006, doi:10.1029/2008GC002171.

Prados, R., R. Garcia, J. Escartín, and L. Neumann (2011), Challenges of close-range underwater optical mapping, in *Oceans 2011*, pp. 1–10, IEEE Press, Piscataway, N. J.

Ramondenc, P., L. N. Germanovich, K. L. Von Damm, and R. P. Lowell (2006), The first measurements of hydrothermal heat output at 9°50′N, East Pacific Rise, *Earth Planet. Sci. Lett.*, *245*, 487–497, doi:10.1016/j.epsl.2006.03.023.

Ruhl, H. A., et al. (2011), Societal need for improved understanding of climate change, anthropogenic impacts, and geo-hazard warning drive development of ocean observatories in European Seas, *Prog. Oceanogr.*, *91*, 1–33, doi:10.1016/j.pocean.2011.05.001.

Sarradin, P. M., J. C. Caprais, R. Riso, R. Kerouel, and A. Aminot (1999), Chemical environment of the hydrothermal mussel communities in the Lucky Strike and Menez Gwen vent fields, Mid Atlantic Ridge, *Cah. Biol. Mar.*, *40*, 93–104.

Sarrazin, J., P. Rodier, M. K. Tivey, A. Schultz, and P.-M. Sarradin (2009), A dual sensor device to estimate fluid flow velocity at diffuse hydrothermal vents, *Deep Sea Res., Part I*, *56*, 2065–2074, doi:10.1016/j.dsr.2009.06.008.

Scheirer, D. S., D. J. Fornari, S. E. Humphris, and S. Lerner (2000), High-resolution seafloor mapping using the DSL-120 sonar system: Quantitative assessment of sidescan and phase-bathymetry data from the Lucky Strike segment of the Mid-Atlantic Ridge, *Mar. Geophys. Res.*, *21*, 121–142, doi:10.1023/A:1004701429848.

Schultz, A., J. R. Delaney, and R. E. McDuff (1992), On the partitioning of heat flux between diffuse and point source seafloor venting, *J. Geophys. Res.*, *97*(B9), 12,299–12,314, doi:10.1029/92JB00889.

Seher, T., S. C. Singh, W. C. Crawford, and J. Escartín (2010a), Upper crustal velocity structure beneath the central Lucky Strike Segment from seismic refraction measurements, *Geochem. Geophys. Geosyst.*, *11*, Q05001, doi:10.1029/2009GC002894.

Seher, T., W. C. Crawford, S. C. Singh, and M. Cannat (2010b), Seismic layer 2A variations in the Lucky Strike segment at the Mid-Atlantic Ridge from reflection measurements, *J. Geophys. Res.*, *115*, B07107, doi:10.1029/2009JB006783.

Simeoni, P., J. Sarrazin, H. Nouzé, P. M. Sarradin, H. Ondréas, C. Scalabrin, and J. M. Sinquin (2007), Victor 6000: new high resolution tools for deep sea research; Module de Mesures en Route, in *Oceans 2007*, p. 133–138, IEEE Press, Piscataway, N. J.

Singh, S. C., W. C. Crawford, H. Carton, T. Seher, V. Combier, M. Cannat, J. P. Canales, D. Dusunur, J. Escartín, and J. M. Miranda (2006), Discovery of a magma chamber and faults beneath a Mid-Atlantic Ridge hydrothermal field, *Nature*, *442*, 1029–1032, doi:10.1038/nature05105.

Spiess, F. N., et al. (1980), East Pacific Rise: Hot springs and geophysical experiments, *Science*, *207*, 1421–1433, doi:10.1126/science.207.4438.1421.

Stein, C. A., and S. Stein (1994), Constraints on hydrothermal heat flux through the oceanic lithosphere from global heat flow, *J. Geophys. Res.*, *99*(B2), 3081–3095, doi:10.1029/93JB02222.

Thatcher, W., and D. P. Hill (1995), A simple model for the fault-generated morphology of slow-spreading mid-ocean ridges, *J. Geophys. Res.*, *100*(B1), 561–570, doi:10.1029/94JB02593.

Tivey, M. A., and H. P. Johnson (2002), Crustal magnetization reveals subsurface structure of Juan de Fuca hydrothermal vent fields, *Geology*, *30*, 979–982, doi:10.1130/0091-7613(2002)030<0979:CMRSSO>2.0.CO;2.

Tolstoy, M., F. Waldhauser, D. R. Bohnenstiehl, R. T. Weekly, and W.-Y. Kim (2008), Seismic identification of along-axis hydrothermal flow on the East Pacific Rise, *Nature*, *451*, 181–184, doi:10.1038/nature06424.

Trivett, D. A., and A. J. I. Williams (1994), Effluent from diffuse hydrothermal venting: 2. Measurement of plumes from diffuse hydrothermal vents at the southern Juan de Fuca Ridge, *J. Geophys. Res.*, *99*(C9), 18,417–18,432, doi:10.1029/94JC00096.

Valentine, D. L., et al. (2010), Asphalt volcanoes as a potential source of methane to late Pleistocene coastal waters, *Nat. Geosci.*, *3*, 345–348, doi:10.1038/ngeo848.

Van Dover, C. L. (2000), *The Ecology of Deep-Sea Hydrothermal Vents*, Princeton Univ. Press, Princeton, N. J.

Veirs, S. R., R. E. McDuff, and F. R. Stahr (2006), Magnitude and variance of near-bottom horizontal heat flux at the Main Endeavour hydrothermal vent field, *Geochem. Geophys. Geosyst.*, *7*, Q02004, doi:10.1029/2005GC000952.

Von Damm, K. L. (1990), Seafloor hydrothermal activity: Black smoker chemistry and chimneys, *Annu. Rev. Earth Planet. Sci.*, *18*, 173–204, doi:10.1146/annurev.ea.18.050190.001133.

Von Damm, K. L., A. M. Bray, L. G. Buttermore, and S. E. Oosting (1998), The geochemical controls on vent fluids from the Lucky Strike vent field, Mid-Atlantic Ridge, *Earth Planet. Sci. Lett.*, *160*, 521–536, doi:10.1016/S0012-821X(98)00108-3.

Wilcock, W. S. D., and J. R. Delaney (1996), Mid-ocean ridge sulfide deposits: Evidence for heat extraction from magma chambers or cracking fronts?, *Earth Planet. Sci. Lett.*, *145*, 49–64, doi:10.1016/S0012-821X(96)00195-1.

Wilson, C., J.-L. Charlou, E. Ludford, G. Klinkhammer, C. Chin, H. Bougault, C. German, K. G. Speer, and M. Palmer (1996), Hydrothermal anomalies in the Lucky Strike segment on the Mid-Atlantic Ridge (37°17′N), *Earth Planet. Sci. Lett.*, *142*, 467–477, doi:10.1016/0012-821X(96)00100-8.